Mathematical Modeling of Vascular Tumor Growth and Development

Michele D. Cooper

Thesis submitted to the faculty of
Virginia Polytechnic Institute and State University
in partial fulfillment of the requirements for the degree of

Master of Science
In
Engineering Mechanics

Ishwar K. Puri
Martin L. Tanaka
Carla V. Finkielstein
Raffaella De Vita

May 12, 2010

Blacksburg, Virginia

Keywords: Mathematical model, Angiogenesis, Vascular tumor, Tumorigenesis

Mathematical Modeling of Vascular Tumor Growth and Development

Michele D. Cooper

Abstract

Mathematical modeling of cancer is of significant interest due to its potential to aid in our understanding of the disease, including investigation into which factors are most important in the progression of cancer. With this knowledge and model different paths of treatment can be examined; (e.g. simulation of different treatment techniques followed by the more costly venture of testing on animal models). Significant work has been done in the field of cancer modeling with models ranging from the more broad systems, avascular tumor models, to smaller systems, models of angiogenic pathways. A preliminary model of a vascularized tumor has been developed; the model is based on fundamental principles of mechanics and will serve as the framework for a more detailed model in the future. The current model is a system of nonlinear partial differential equations (PDEs) separated into two basic sub-models, avascular and angiogenesis. The avascular sub-model is primarily based of Fickian diffusion of nutrients into the tumor. While the angiogenesis sub-model is based on the diffusion and chemotaxis of active sprout tips into the tumor. These two portions of the models allow the effects of microvessels on nutrient concentration within the tumor, as well as the effect of the tumor in driving angiogenesis, to be examined. The results of the model have been compared to experimental measurements of tumor growth over time in animal models, and have been found to be in good agreement with a correlation coefficient of (r^2=0.98).

Acknowledgements

I wanted to express my deepest gratitude to Dr. Ishwar Puri for giving me the opportunity to work with him. His guidance and enthusiasm for research has greatly helped me during my learning process; through his encouragement and enthusiasm my own interests have become more engaged. I would also like to thank Dr. Martin Tanaka for his help and support through this process. Despite the distance, he has been extremely willing to help and very encouraging as well. My thanks also goes out to Dr. Rafaella DeVita and Dr. Carla Finkielstein for serving as my committee members.

I would also like to thank my husband Dan for all his support.

Table of Contents

List of Figures

List of Tables

Chapter 1 Introduction

1.1 Impact of Cancer

Cancer is one of the leading causes of death in the United States, second only to cardiovascular disease and, responsible for an estimated 562,340 deaths and 1,479,350 new cases diagnosed in 2009[1]. The treatment of cancer had a financial impact of approximately $228.1 billion USD[1]. These statistics present a clear human and financial need for the development of new treatments for cancer, which is hindered by the fact that cancer is a group of many different diseases. As a result, while research into other diseases such as cardiovascular disease can be focused on several key areas, cancer research must be spread out among many different diseases. This greatly increases the volume of cancer research that needs to be performed, which is both expensive and time consuming. Accurate mathematical models of cancer can greatly increase the efficiency of cancer research by allowing some experiments to be replaced by simulations, and by suggesting directions for experimental research to be performed.

Examination of cancer statistics demonstrates that most cancer deaths are associated with vascular tumors, which have developed capillary beds through the process of angiogenesis[1]. However, mathematical models of tumors have primarily focused on the avascular types, which have not developed such capillary beds, and are limited in size by the nutrient supply which can diffuse into the tumor from surrounding tissues. This provides the motivation for this work. A tumor model of vascular tumor growth has been developed based upon prior models of angiogenesis and tumorigenesis[2, 3]. The behavior of this model has been studied and compared with experimental results, which demonstrates the validity of the model.

1.2 The Six Hallmarks of Cancer

This section involves a brief discussion of the six different hallmarks of cancer, listed in **Error! Reference source not found.** with the purpose of introducing the basic biology of the problem. The section draws heavily from a review article by Hanahan and Weinberg[4]. As seen in this section, the term cancer represents many separate diseases, which possess six common attributes:

1. Self-sufficiency in growth signals
2. Insensitivity to anti-growth signals
3. Limitless replicative potential
4. Evasion of apoptosis
5. Sustained angiogenesis
6. Tissue invasion & metastasis

Each of these attributes is briefly discussed separately below.

1.2.1 Self-sufficiency in growth signals

Normal cells require mitogenic growth signals before they can move into the proliferative state from the hypoxic state. These growth signals pass through transmembrane receptors to bind with specific signaling molecules (e.g. diffusible growth factors, extracellular matrix components, and cell-to-cell adhesion/interaction molecules). Tumor cells have developed ways to bypass the normal system that requires mitogenic growth signals to change to proliferative state. Three common strategies exist for reaching this state of autonomy, (1) altering extracellular growth signals, (2) altering transcellular transducers of the growth signals, and (3) altering the intracellular circuits that translate growth signals into action. The alteration of extracellular growth signals leading to self-sufficiency can occur in many ways, one of which is that the receptor overexpression can cause a hypersensitivity to growth factors in the tumor cells which would cause proliferation at much lower levels[5]. Also tumor cells can express different types of extracellular matrix receptors and this can be changed in favor of receptors that produce progrowth signals[6, 7]. The intracellular circuits can be altered as well, the SOS-Ras-Raf-MAPK

cascade can be altered so a structurally altered Ras protein will release mitogenic signals without receiving any stimulation by its normal upstream regulators[8].

1.2.2 Insensitivity to anti-growth signals

Within a normal tissue, many anti-proliferative signals work to maintain tissue homeostasis; these signals (soluble growth inhibitors and immobilized inhibitors) are found in the extracellular matrix and on the surfaces of nearby cells. The growth-inhibitory signals are received by transmembrane cell surface receptors attached to intracellular signaling circuits, which lead to a sensitivity to anti-growth signals[9]. Two mechanisms exist to block anti-growth signals, (1) cells avoid being forced into a state of hypoxia (G_0 state which cells can leave at a later time when appropriate to proliferate) or (2) cells avoid being forced to enter the post-mitotic state (e.g. cells can no longer proliferate). The signals corresponding to the first mechanism almost universally work through retinoblastoma protein pRb; disruption of the pRb pathway therefore renders the cell insensitive to such anti-growth signals. The molecular biology involved with the second pathway is not well understood, but may involve the c-myc oncogene, overexpression of which may reverse cellular senescence[9].

1.2.3 Evading apoptosis

Apoptosis, otherwise known as cell-mediated death, is initiated when a cell develops a mutation that is deemed harmful by the body. Apoptosis begins with the disruption or lysing of the cell membrane; next, the cytoplasmic and nuclear skeletons are degraded and lastly the chromosomes and nucleus are broken down. This process occurs within the range of approximately 30-120 minutes. In the end, the remnants of the apoptosis process are absorbed by nearby cells usually within 24 hours[10]. Three different mechanisms exist that aid tumor cells in evading apoptosis, (1) inhibition of the cellular signal from being sent, (2) overcoming apoptosis signals with anti-apoptosis signals, and (3) blocking apoptosis signals. There are several different ways to inhibit the cellular signal from being sent, most of

those involve the inhibition or the mutation of the p53 tumor suppressor gene. The inactivation of the p53 gene, seen in 50% of human cancers, can result from the removal of an important part of the DNA damage sensor which effectively inhibits the DNA damage sensor's ability to induce the apoptotic effector cascade[11]. An alternate method of evading apoptosis is to suppress the apoptosis signal by emitting more anti-apoptosis signals. The PI3 kinase-AKT/PKB pathway is responsible for sending out anti-apoptosis signals; several ways this pathway can be activated by extracellular factors (IGF-1/2 or IL-3) [citation Evan and Littlewood, 1998], by intracellular signals (from Ras)[12], and loss of the pTEN tumor suppressor[13]. The last mechanism for evading apoptosis, blocking the signal, stems from the removal of the FAS death signal[14].

1.2.4 Limitless replicative potential

Normal cells (excluding stem cells) have limited replicative potential[15]; generally, cell populations replicate a certain number of times and then enter a senescent phase. Cells remain in this phase until its pRb and p53 tumor suppressor proteins are disabled and then they can multiply again until they entire a crisis state, characterized by massive cell death[16]. Tumor cells differ from normal cells because they appear to be immortal which suggests that the acquisition of limitless replicative potential is essential for malignant tumor growth[15]. Two mechanisms exist to explain the acquisition of limitless replicative potential, (1) telomere maintenance and (2) the circumvention of cellular senescence. Telomere maintenance is present in almost all types of malignant cells[17] and the most common method of maintenance (85-90% of all tumors) is by increasing the activity of the telomerase enzyme[18]. The second mechanism is more uncertain at this time; however, the circumvention of the cellular senescence is another possibility because the senescent state acts as a protective mechanism that can be activated by shortened telomeres or conflicting growth signals which will force cells into a G_0 like state[19].

1.2.5 Sustained angiogenesis

Angiogenesis is the growth of new blood vessels within the human body; this process is transient and carefully regulated. Tumor cells initially lack the ability to sustain angiogenesis, thereby limiting growth, which encourages the adaptation to develop this ability[9, 20, 21]. Experimental evidence shows sustained angiogenesis to be critical for the progression of tumor growth; Kim et al. used anti-VEGF antibodies to impair neovascularization and growth of subcutaneous tumors in mice [22], and Millauer et al. used a dominant-interfering version of the VEGF receptor 2 to impair neovascularization and tumor growth[23]. Sustained angiogenesis is critical to tumor growth and progression and primary mechanism for obtaining this ability is to manipulate the positive and negative signals that initiate or block angiogenesis[9]. Common methods of achieving sustained angiogenesis can be achieved by one or more of the following, (1) increasing VEGF/FGF concentrations, (2) expressing endogenous inhibitors, and (3) decreasing β-interferon [24].

1.2.6 Tissue invasion and metastasis

Metastases, tumors that grow in different location in the body from the primary tumor, cause 90% of human cancer deaths[25]. Metastasis is not clearly understood but there are two proposed mechanisms that enable this process, (1) interruption of CAMs and integrins and (2) changes in extracellular proteases. Cell-cell adhesion molecules (CAMs) facilitate cell-cell interactions and integrins link cells to the extracellular matrix. A commonly seen mutation for this particular mechanism is in E-cadherin. The E-cadherin couples adjacent cells and promotes the transmission of antigrowth and other signals, these functions are lost in most epithelial cancers by the inactivation of E-cadherin or β-catenin genes, transcriptional repression, or proteolysis of the extracellular cadherin domain[26]. The second mechanism involves the extracellular proteases; often many types of carcinomas utilize stromal and inflammatory cells' ability to produce matrix-degrading proteases[27].

1.2 Tumor Stages

1.2.1 Avascular

In many cases, a tumor may possess self-sufficiency with regard to growth signals, insensitivity to anti-growth signals, the ability to evade apoptosis, and unlimited replicative potential, yet still remain relatively small in size and present little threat to the patient. The reason for this is that nutrients are only able to diffuse a very short distance from capillaries in sufficient quantity to support cellular metabolism. Since tumors have no native capillary blood supply, an avascular tumor reaches a finite size that is maintained. Proliferation of the tumor cells in the outer regions of the tumor (which are well supplied with nutrients by diffusion from outside the tumor) is balanced by cell apoptosis and the degradation of dead cells within the center of the tumor. In addition, without a blood supply, the likelihood of the tumor spreading to other regions of the body is extremely low. Due to the combination of small size and low likelihood of metastasis, the threat posed by such tumors is considered low, and the primary risk associated with such tumors is that the tumor may develop the ability to initiate angiogenesis and metastasize, becoming a vascular tumor.

1.2.2 Vascular

These limitations which act on avascular tumors illustrate the vital importance of angiogenesis in tumor growth. Once the process of angiogenesis has been initiated, capillaries will sprout from blood vessels near the tumor, and invade into the tumor. This has the affect of providing a direct supply of nutrients to the tumor, decreasing the dependence on the diffusion of nutrients from regions outside the tumor. This effectively removes one of the last limits on the tumors size, the previously discussed cell death due to extreme hypoxia in the central regions of the tumor, since there is now a mechanism for changing hypoxic and necrotic cells back to proliferative behavior. However, in some tumors, this process performs poorly, and the capillary beds that form are ‘leaky’, which hinders the supply of

nutrients to the tumor, leading to tumor remain avascular in behavior. In many tumors, however, these capillary beds manage to successfully provide nutrients to the tumor, paving the way for greatly increased tumor growth. Angiogenesis also paves the way for the final hallmark of cancer, which is metastasis. Once the tumor has become vascularized, tumor cells may slough off into the blood stream, landing at far removed locations within the body initiating growth of secondary tumors. Metastasis remains one of the worst prognoses in oncology, since it makes treatment of cancer extremely difficult, usually negating the use of all treatments except chemotherapy, which is very harmful to the patient.

1.3 Research Objectives

Although the mathematical models of the tumor growth and development have existed for many years, the vast majority of the work in the field has focused on the modeling of avascular tumor growth. However, as previously discussed, these represent the safest class of tumors, since tumor growth is limited by its nutrient supply. Far more clinically significant are those tumors whose dependence upon nutrient diffusion from outside the tumor is greatly reduced due to an internal vascular supply (e.g. vascular tumors).

In this study, a mathematical model has been developed to describe the growth and development of these tumors. A major goal of the model was to examine the interaction between the growth of the tumor and the invasion of capillaries into the tumor, forming tumor beds. Towards this end, the development of the model started by identifying previously existing models of both avascular tumor growth as well as the process of angiogenesis, independent of any affects from a growing tumor. Two such models were coupled to consider the influence of angiogenesis on the nutrient concentration within the tumor, and the role of tumor hypoxia in driving the initiation of angiogenesis. The end result of these additions was a continuum based model that coupled the two processes to solve for the growth of a vascular tumor over time.

Once the model was formulated, several different types of analysis were performed to examine the function of the model. Sensitivity studies were performed to examine the rate of change of the solution to small perturbations in the model parameters. Similarly, to examine the influence of highly nonlinear terms, a parametric study was performed which examined the influence of much larger changes in the model parameters on the model solution. Finally, experimental data for the growth of pancreatic tumors implanted in mice was obtained and an optimization scheme was run to determine the set of model parameters which resulted in the best fit with the experimental data[28]. The results showed that a very high level of correlation (r^2=0.98) was achieved between the experimental data and the model predictions, lending strong evidence to the validity of the model.

Chapter 2 Literature Review

Mathematical models have been developed to describe many phenomena in countless different fields. Mathematical models can increase fundamental understanding of a phenomenon by demonstrating the feasibility of various hypotheses to describe the phenomena. In addition, they can allow simulations of experiments that are either impractical or impossible to be performed . They are extremely useful for making predictions about real world phenomena and are vitally important in the development of control models. For these reasons and more, there has been a great depth and breadth of research into the mathematical modeling of tumor growth and development. Previously developed models have been used to examine the affects of different chemotherapeutic treatments on tumor growth[29, 30], while others have examined the validity of the stem cell hypothesis[31]. For the purposes of this paper, prior art is divided up into three main categories. First, the development of models of various types seeking to describe the growth of a tumor, known as tumorigenesis, is discussed. A second section discusses the development of models for the process of angiogenesis, in which new blood vessels develop and grow towards the tumor in response to oxygen starvation signals

originating from within the tumor. As previously discussed, this is the vital step in the development of clinically dangerous tumors. Finally, the last section discussion prior works that have attempted to model the coupled growth of vascular tumors, combining the processes of tumorigenesis with the process of angiogenesis. It is in this area that the contributions of the present work exist.

2.1 Tumorigenesis Models

2.1.1 Continuum Models

As early as 1928, it was recognized from Hill's work that the diffusion of nutrients played a vital role in many physiological processes, including the growth and development of tumors[32]. However, much of the early mathematical modeling work, prior to the 1950s was focused solely on the development of curves that matched observed growth and determining the mathematical characteristics of tumor growth[33, 34]. This early work showed that tumor growth, like many growth phenomena, could be fit over a large region by the Gompertzian equation, which exhibits exponential retardation. However, experimentally observed growth ultimately becomes linear. The first mathematical model considering the balance of oxygen consumption and diffusion was proposed by Thompson and Gray, based on the observations of Hill as well as the existence of necrotic core with tumors. This model demonstrated that the observed behavior was on the scale that would be predicted if tumor growth were governed by oxygen metabolism[35].

The first complete model of tumorigenesis, however, coupling the diffusion of oxygen with the growth of tumor was proposed by Burton in 1966. A key feature of this model was the existence of a thin shell of proliferating cells surrounding a large core of nonreproductive hypoxic and necrotic cells, resulting in reduced growth rates due to reduced reproductive fraction, ultimately producing the experimentally observed linear growth[36]. A uniformly, highly vascular region was assumed to exist outside of the tumor. This model was extended by Greenspan, who introduced the concept of a surface

tension, the net effect of which was to replace tissue volume lost to necrosis by the inward motion of cells from the outer proliferative region[37]. This is a common component of current models of avascular tumorigenesis. However, experiments by Sutherland and Durand suggested that cell necrosis alone could not be responsible for the total diminishment of tumor growth rate[38, 39]. The work of Kerr, which showed that apoptosis can always be detected in tumors, suggested that the missing process was apoptosis[40]. McElwain and Morris applied these findings into a new model, in which two mechanisms of cell death occur, necrosis, where the cell remnants decay over time, and apoptosis, or controlled cell death, which results in rapid removal of cellular remains[41]. This tumor model represents the basis of most continuum based modern tumorigenesis models[42], with three distinct regions: a outer proliferative region, superficial to a hypoxic shell, and finally an innermost necrotic core.

2.1.2 Discrete Models

Another body of literature has focused on modeling tumor behavior at the cellular level using cellular automaton models. These models vary significantly in form from the previously mentioned continuum models. While continuum models are formulated using ordinary and partial differential equations, cellular automaton models consist of lattice networks, discrete states, and sets of governing rules. While not as immediately applicable to the development of the current model, there is interplay between tissue scale and cellular level modeling, with each aiding the advancement of the other. As a result, it is worthwhile to briefly discuss such cellular models.

Cellular automata are discrete models consisting of a regular grid of cells, each of which has a finite number of states. The value of these states is allowed to change over time in accordance to some predefined rules. These models are ideally suited for the modeling of phenomena which do not lend themselves to a continuum description, particularly those systems under non-deterministic (stochastic) influences. For example, the growth of an individual capillary under the influences of both chemotaxis and random diffusion is easily studied using such a model. Cells are created over the domain of interest,

and the state of these cells represents the presence/absence of the capillary. However, the computational requirements for such models grow quickly with domain size, making them difficulty at best to implement in many real world problems. Despite this limitation, they remain a useful tool for examining and modeling specific aspects of tumorigenesis, even if the entire tumor cannot be reasonably modeled.

One of the earliest CA models is that of Düchting, published in 1978. The model allowed simulation of competition between ordinary (healthy) cells along with rapidly proliferating malignant cells, considering only mitosis and cell death, without examining contributing factors[44]. Surgical removal of cell bodies was also considered. This work was limited by computational power at the time to only using a 10x10 network, resulting in a model that can only be applied for very small tumors in early stages of development. Follow up works extended the model to a 100x100 network and later a 3-D 40x40x40 network[45, 46].

More recent efforts have tried to more accurately model macroscopic phenomena using cellular automaton models based upon microscropic behavior[47]. Kansal et al. published such a 3-D probabilitistic model of brain tumor growth[48, 49]. Similar to continuum models, this model contained three separate types of cells, proliferative, hypoxic, and necrotic. One of the unique features of this model compared to other such models is that the lattice network is not regular. Instead, the density of the network varies considerably, being more dense in the center of the tumor, with each site representing a different number of cells. Unlike the previously discussed model, this model has been validated by comparison with experimental results (such results did not exist at the time of Düchting's model[47]). Another model with a similar goal of reproducing macroscopic results is the 2-D model of Dorman and Deutsch[50]. This model was self-organizing, and consists of two separate cell types, tumor and necrotic cells, with both nutrients and a chemotactic signal from necrotic cells being represented by continuous fields. Cells were allowed to undergo mitosis, apoptosis, and necrosis. One of the major

achievements of this model is its ability to generate the layered geometry previously discussed, which is both clinically observed and predicted by continuum models. Another self organizing avascular tumor model was proposed by Dresden[51].

2.1.3 Multiscale

In general, continuum models can be solved with much less expense that discretized cellular automaton models, due to the need of cellular automaton models to account for every cell (or small groups of cells) within the tumor. However, there are details of cellular behavior that are most easily accounted for through the use of cellular models. As a result, in recent years there has been an increase in the development of multiscale models of tumorigenesis. Such models have the potential to combine the efficiency of continuum models with the ability of cellular automaton models to describe the microenvironment surrounding cells. One such model is that of Jiang et al, which consists of a Boolean network governing activity at the sub-cellular level (ex. protein expression), a lattice network at the cellular level, and reaction-diffusion partial differential equations at the tissue level to determine concentrations of nutrients, growth factors, and inhibitors[52]. An advantage of such models is that they allow examination of micro-environmental effects on the macroscopic behavior. Indeed, one of the primary results of this study was an examination of the micro-environmental environment required for tumor cell survival and macroscopic tumor growth. More significantly, much of the prior work developing models for vascular tumors involves this type of model, hence, this will be a major focus of the section on vascular tumor models.

2.2 Angiogenesis Models

Angiogenesis is the process of developing new blood vessels, this normally occurs as part of the wound healing response, and is also a response to tissue hypoxia. Tumor-induced angiogenesis is a vital phase of the growth of a tumor, without which the tumor cannot grow much beyond about 2mm in

diameter[3]. Unlike tumorigenesis, early work in the mathematical modeling of angiogenesis has been divided between continuum and discrete models. While continuum models are more efficiently solved, they do not provide the details of capillary network formation that discrete models can, albeit at significant expense.

2.2.1 Continuum

The earliest example of a continuum model of angiogenesis is the work of Zawicki et al[53]. This model consisted of three partial differential equations governing erythrocytes, tissue cells, and vessel cells. However, the model neglected interaction between the three species, since it was not yet determined which growth factors contributed to endothelial cell migration and proliferation. Chemotaxis was also neglected. A later model was developed by Balding and McElwain, who were attempting to describe angiogenesis in the cornea (which reduced the dimensionality of the problem to 2-D). They developed a novel appropach of treating sprout tip density (concentration), measured in units of tips per unit volume/area separately from the location of capillaries density, measured in units of length per unit volume/area[54]. The rate at which capillary is laid down is calculated by the flux of sprout tips through a region. This approach has several important advantages. It can account for the experimental observation that most reproduction of endothelial cells in angiogenesis occurs at the sprout tip. It also can account for anastomosis (the closing of flow loops in the capillary network) and braching. Previous works by Orme and Chaplain have implemented this approach for 1-D geometries, accounting also for the affects of tumor angiogenic factor (TAF)[55, 56]. Orme and Chaplain's model consists of the series of partial differential equations shown below, where *n(x,t)* corresponds to the sprout tip concentration, *ρ(x,t)* concentration of capillary length, and *c(x,t)* corresponds to the concentration of TAF:

$$\frac{\partial n}{\partial t} = \frac{\partial}{\partial x}\left[D\frac{\partial n}{\partial x} - n\chi\frac{\partial c}{\partial x}\right] + a_0\rho c + a_1 H(c-\vartheta)nc - \beta n\rho \qquad (1)$$

$$\frac{\partial \rho}{\partial t} = D\frac{\partial n}{\partial x} - n\chi\frac{\partial c}{\partial x} - \gamma\rho \tag{2}$$

$$\frac{\partial c}{\partial t} = \frac{\partial^2 c}{\partial x^2} - \lambda c - a_1 H\left(c - \vartheta\right)nc \tag{3}$$

In the equation governing the rate of change of sprout tips (*∂n/∂t),* the first term corresponds to the migration/diffusion of sprout tips, the seconds term corresponds to the branching of sprout tips, the third corresponds to proliferation, and the last term corresponds to the loss of tip concentration due to anastomosis. This model has some shortcomings, particularly with regard to extension to higher order geometries (2-D and 3-D), nevertheless, it represents a major advancement in the ability to model angiogenesis using a continuous model. A later model by Orme and Chaplain extended the body of work by including the effects of haptotaxis (migration in response to fibrin released by other capillaries) in addition to those of chemotaxis[57, 58].

One of the most commonly cited models however, is that of Anderson and Chaplain, who derived a 1-D model describing the motion of endothelial cells, followed soon after by a series of 2-D models[59-61]. Anderson and Chaplain's models neglected proliferation, but considered haptotaxis as well as chemotaxis, which was considered to be nonlinear, on the hypothesis that cells failed to reach the center of the tumor due to insensitivity of cells to high levels of TAF. The model consisted of three partial differential equations representing the rate of change of endothelial cell concentration, *n,* TAF concentration, *c,* and fibronectin concentration, *ρ*:

$$\frac{\partial n}{\partial t} = \nabla \bullet \left[D\nabla n - n\left(\frac{\chi}{1+ac}\nabla c + \rho\nabla f \right) \right] \tag{4}$$

$$\frac{\partial c}{\partial t} = -\eta nc \tag{5}$$

$$\frac{\partial \rho}{\partial t} = \beta n - \gamma n f \tag{6}$$

Like other earlier work, this model neglects the effects of inhibitors of angiogenesis, since some of the most important inhibitors were not discovered until the late 1990s[62]. Later works by Anderson and Levine examined the affects of inhibitors, in particular with regard to the initiation of angiogenesis[63-65]. More importantly, the model does have some disagreements with clinical and experimental observations. For example, even without proliferation, in some circumstances the model predicts complete angiogenesis (capillaries reach the center of the tumor) under certain circumstances, which stands in contrast with the experimental results of Ausprunk and Folkman[66]. In addition the model predicts slowing vascularization as capillaries approach the tumor (vascularization within a tumor was not considered), which is against in constrast with experimental results of Folkman[67]. Despite these shortcomings, this model has become the basis for much of the current work modeling angiogenesis. By making the assumption that sprout tips diffuse similarily to an endothelial cell (a relatively common assumption), one can apply the previously discussed concepts of sprout tip and capillary concentrations to the model of Anderson and Chaplain.

Other models have expanded upon the description of the effects of the extracellular matrix, which in Anderson and Chaplain's work is lumped into the fibronectin/haptotaxis term. Such models generally retain the form of the previously discussed continuum models, but add an additional term accounting for the movement of endothelial cells due to the local deformations in the extracellular matrix[62]. Such models have been developed by Murray and Swanson, as well as Holmes and Sleeman[68, 69]. The model by Holmes and Sleeman consisted of equations governing endothelial cells, TAF, fibronectin, and the extracellular matrix, but neglected any effects of inhibitors.

2.2.2 Discrete

The role of discrete modeling with regard to angiogenesis is even more significant than it is for tumorigenesis. This is primarily due to the substantial complexity of the process of angiogenesis, even at the cellular level. One of the first such models is that of Stokes and Lauffenburger[70]. This model considers individual sprout tips, and uses a stochastic differential equation to govern the velocity of the sprout tip over time. These differential equations consist of a damping term, a random term, and a chemotaxic term (a steady state TAF gradient was assumed). Branching occurred in the model with a certain probability, which increases as the tip approaches the tumor, and anastomosis was considered to occur when two sprout tips came within the diameter of a single cell, in which case one sprout tip was removed from the population. However, there are several issues with this model. The treatment of branching is purely phenomenological and does not produce the experimentally predicted "brush-border" affect, where pronounced branching occurs as capillaries get near the tumor. In addition, the model does not consider the inhibition of angiogenesis, which had not been properly described at the date of publication.

A somewhat more recent (and entirely separate) model is that of Anderson and Chaplain, who developed a discretized cellular automaton model of their previously discussed continuous model[60, 61]. These partial differential equations were discretized, and the results were used to determine the probabilities that an endothelial cell at a given location in the domain would move to a different (adjacent) grid point in the next time step. Hence, the motion of endothelial cells is based upon the processes of (random) diffusion, chemotaxis, and haptotaxis, as is the case in the discrete model, resulting in a biased random walk. In this respect, the model shares similarities with the prior model of Othmer and Stevens, which consisted of equations (discrete in time and continuous in space) governing the probability of a cell's location under chemical stimulus[71].

Similar to the work of Stokes and Lauffenburger, branching is accounted for through the use of a probability, which increases as the sprout approaches the tumor. Their treatment of anastomosis is similar as well, but complicated by rules requiring a vessel to progress a certain defined distance from the vessel before anastomosis is possible, to match the experimental results of Paweletz and Knierim[72]. Nevertheless, the results match those observed experimentally both *in vivo* and *in vitro,* including the existence of a brushed border,consisting of many capillaries jumbled closely together due to rapid branching. Due to the complexity of the process of angiogenesis, accounting for additional affects within these models, and the derivation of other models, remains an active area of research, nevertheless, much current work is based on the expansion and analysis of this original model derived by Anderson and Chaplain.

2.3 Vascular Tumor Models

While a large body of work has been accomplished in the modeling of tumorigenesis and angiogenesis individually, modeling the development of vascular tumors by necessity requires modeling the interplay between the two. Angiogenesis is driven by the development of hypoxic regions developing as a tumor grows through its avascular phase. Similarly tumor growth beyond an avascular size depends upon the additional nutrients obtained through (partially) successful angiogenesis. Here the body of work is substantially smaller than the corresponding bodies of work for angiogenesis and tumorigenesis individually. Much of the work in this area has been in the form of cellular automaton models, as well as continuum models.

One such early work using cellular automaton models is that of Patel et al.[73]. However, this model does not model angiogenesis, rather its goal is studying the effects of native tissue vascularity (vessels existing prior to the development of the tumor) on the growth and development of an otherwise avascular tumor. As a result, the model does not include an angiogenesis model. A similar

statement can be made regarding the continuum model proposed by Hahnfeldt et al.[74]. This model was developed primarily to model the effects of angiogenesis inhibitors on tumor growth, but nevertheless does not include a mechanistic angiogenesis model, although it does contain a continuum tumor model based upon the diffusion of tumor cells. This demonstrates a trend in vascular tumor modeling. Much of the work that is being done has had as its primary focus examining the effects of drugs and other inhibitors, rather than fundamentally modeling mechanistically the process of vascular tumor growth and development[29, 75-77]. This body of work also includes work examining the behavior at the microscopic/cellular scale[78].

More recent works have combined aspects from previously developed models to form continuum models of vascular tumor growth. Zheng et al. developed a coupled model, using a level set approach, where the tumor cells were divided into two populations, necrotic and viable, and were modeled as a viscous fluid in a porous space. Angiogenesis was modeled using a discrete model following that of Anderson and Chaplain. The resulting model was solved using adaptive finite element schemes, due to its complex nature, with the concentration field being dependent upon the exact capillary configuration at that point in time, with capillaries being treated as sources of nutrient concentration. Hogea et al. built upon this model, performing simulations on 2-D and spherical geometries[79]. Here, the affects of increased capillary count due to angiogenesis was modeled through an increased nutrient diffusivity, an approach that has been utilized in other models[3]. Frieboes et al. took a similar approach of coupled models, coupling a mixture model of tumorigenesis with the angiogenesis model of Planck and Sleeman[80]. Most recently, Macklin et al. developed a multiscale model, based upon previous literature, that accounts for the effects of blood flow within the capillaries, and the effects of this flow upon the capillary network. However, lacking in this body of literature, are relatively simple mechanistic models that couple the processes of tumorigenesis and angiogenesis, which would allow predictions of vascular tumor growth

Chapter 3 Theoretical Model

3.1 Model Overview

The mathematical model developed in this work consists of two coupled sub-models, one which governs the growth of the tumor, referred to as the tumorigenesis sub-model, and another that describes the progression of angiogenesis. The starting point for the formulation of the tumorigenesis sub-model is the continuum model for avascular tumorigenesis of gliomas developed by Tanaka et al, which in turn builds upon the body of previous work developing continuum models of tumorigenesis[3]. The angiogenesis sub-model builds upon the work of Anderson and Chaplain, as well as Balding and McElwain[54, 60]. The equations for both sub-models are derived for a spherically symmetric geometry. A high level overview of the model is shown in Figure 1.

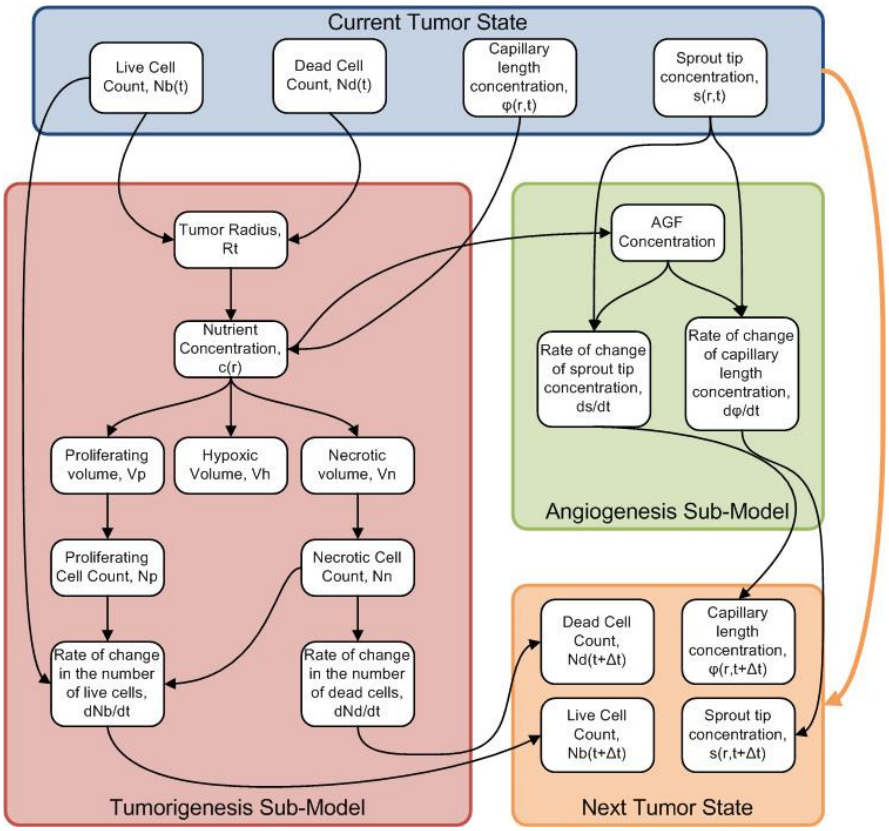

Figure 1: High-level overview of the model. Note that the coupling occurs from the use of capillary length density, *φ,* in the Tumorigenesis sub-model and the use of tumor radius in the angiogenesis sub-model.

The primary variables of the tumorigenesis sub-model are the number of live cells present in the tumor, $N_b(t)$ and the number of dead cells, $N_d(t)$. In this sub-model there are several simplifying assumptions. First, a constant tumor cell size is assumed, and it is assumed that there are no voids or gaps within the tumor volume; the tumor represents a solid mass of cells. Second, diffusion of nutrients is assumed to be quasi-steady, so that a (different) steady state solution can be applied at each time step. This assumption is justifiable based since the diffusivity of nutrients is much larger than the proliferation rate of cells.

The angiogenesis sub-model uses concepts from Balding and McElwain, who represented capillary development in terms of two separate variables, a sprout tip concentration, $s(r,t)$, which has units of sprouts per unit volume, and capillary length concentration, $\varphi(r,t)$, with units of length (of capillary) per unit volume. As a result, these two field variables represent the dependent variables of the angiogenesis sub-model. Again, simplifying assumptions were made in the angiogenesis sub-model, as was the case with the tumorigenesis sub-model. Diffusion of angiogenic growth factor (AGF) was assumed to be quasi-steady, analogous to the treatment of nutrient diffusion in the tumorigenesis sub-model; this was done by the same argument. In addition, departing from the work of Anderson and Chaplain, chemotaxis here was assumed to be linear for computational efficiency as well as simplicity, and haptotaxis was neglected. The justification for the last assumption arises from the physical role of haptotaxis, which is to draw capillaries together to form flow loops, known as anastomosis. In this spherically symmetric model, there are no gradients in the angular (non-radial) directions to cause sprout tip movement, thus the model does not account for the anastomosis.

The remainder of this chapter is broken into three sections. First, the tumorigenesis model is described in great detail. The original model presented by Tanaka et al. is described first, after which the additions to the model to make it valid for use in a vascular tumor (as opposed to the avascular tumor

for which it was initially derived) will be presented. Similarly, in the second section, the angiogenesis model derived by Anderson and Chaplain will be presented, and then the additions to the model to make it useful in the context of a vascular tumor will be presented. Finally, the numerical methods used to solve the model will be presented, starting with the methods used to discretize the model in space, followed by the methods used to integrate the equations in time.

3.2 Tumorigenesis Sub-model

3.2.1 Avascular Glioma Model (Tanaka et al.[3])

Diffusion and Nutrient Concentration

Due to the limitless replicative potential, self-sufficiency with regard to growth signals, a partial ability to avoid apoptosis, and insensitivity to anti-growth signals, which are hallmarks of cancer, the proliferation of tumor cells is primarily governed by the availability of nutrients. Hence, this model, like most such models is build around the diffusion of nutrients into the tumor, whose radius can be calculated from the number of live and dead cells:

$$R_T = R_C (N_b + N_d)^{1/3} \tag{7}$$

where R_c represents the radius of a tumor cell. Within the tumor the rate of change of nutrient concentration, c, at any given point depends upon the balance of two terms, Fickian diffusion the metabolic usage of nutrients. Because nutrient diffusion is considered to be at quasi-steady state, the time derivative of nutrient concentration is everywhere zero.

$$\frac{\partial c}{\partial t} = D_c \nabla^2 c - S = 0 \tag{8}$$

where D_c is the diffusivity of the nutrient. Applying the form of the Del operator in spherical coordinates, the following is obtained:

$$\frac{D_c}{r^2}\frac{d}{dr}\left(r^2\frac{dc}{dr}\right)-S=0 \tag{9}$$

which can be directly integrated to obtain the general form of the solution. The outer boundary condition is considered to be a constant concentration c_0, while the inner boundary condition is zero concentration gradient, applied at some location to be determined, defined here as α:

$$\begin{aligned} c(R_T) &= c_0 \\ \left.\frac{dc}{dr}\right|_{r=\alpha} &= 0 \end{aligned} \tag{10}$$

If the tumor is sufficiently small, α=0. However, as the tumor grows larger, it will eventually reach a size where concentration in a central region is uniformly zero, all available nutrients have been consumed by outer regions of tumor. This begins to happen at a threshold radius, R_{th}, defined by:

$$R_{Th}=\sqrt{\frac{6Dc_0}{S}} \tag{11}$$

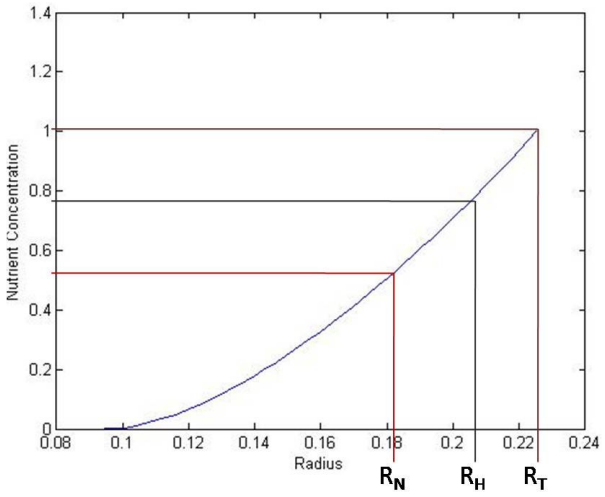

Figure 2: Example nutrient concentration profile. Locations of the necrotic threshold radius r_n and the hypoxic threshold radius r_h are shown.

For tumors larger than this, the value of α must be calculated, therefore an additional piece of information is required to solve the equations. This additional condition is that the concentration at $r=\alpha$ is zero.

$$c(\alpha) = 0 \tag{12}$$

With this additional condition, it becomes possible to solve for all undetermined coefficients in the general solution, including α. Once the concentration profile *c(r)* has been obtained, the next step is to determine the locations within the tumor where the concentration reaches certain threshold values, which divide the live cell population into three conditions, proliferating cells that have sufficient nutrient supply to undergo mitosis, hypoxic cells that cannot reproduce, but remain alive in a quiescent state, and necrotic cells that are dying due to nutrient starvation. Specifically of interest are the radii where the concentration is at the hypoxic threshold value r_h which is the minimum concentration beyond which cells are hypoxic and those actively proliferating, and r_n, which represent the minimum concentration at which hypoxic cells are able to survive in a quiescent state and avoid undergoing necrosis. These values are represented graphically in Figure 2. The concentration profile may be used to solve numerically using root finding methods to obtain these two radii, according to equation 13:

$$\begin{aligned} c(r_h) - c_h &= 0 \\ c(r_n) - c_n &= 0 \end{aligned} \tag{13}$$

Note that in some cases these radii may not be reached. For a very small tumor, all cells in the tumor will receive sufficient nutrients to proliferate and both r_h and r_n will be zero. For a slightly larger tumor r_h will have a non-zero value while r_n will remain zero. Finally, for a sufficiently large tumor that contains all three cell conditions, both r_h and r_n will be non-zero. Once these radii values have been obtained, it is possible to obtain the tumor volume containing cells of each condition:

$$V_n = \frac{4}{3}\pi r_n^3$$
$$V_h = \frac{4}{3}\pi r_h^3 - V_n$$
$$V_p = \frac{4}{3}\pi R_T^3 - V_h - V_n \qquad (14)$$

Once these volumes have been determined, the number of proliferating cells and the number of necrotic cells can be calculated:

$$N_P = \left(V_p / V_T\right)\left(N_b + N_d\right)$$

$$N_n = \left(V_n / V_T\right)\left(N_b + N_d\right) - N_d \qquad (15)$$

where V_T represents the total volume of the tumor. The subtraction of the dead cell count in the equation for the number of necrotic cells represents the assumption that all dead cells within the tumor are within the necrotic region. This assumption is reasonable in light of the mechanism by which dead cells are created. Having calculated the number of proliferating and necrotic cells present in the tumor, it is possible to calculate the rate of change in the number of live and dead cells:

$$dN_b/dt = \omega_p N_p - \omega_a N_b - \omega_n N_n \qquad (16a)$$

$$dN_d/dt = \omega_n N_n - \omega_d N_d \qquad (16b)$$

where ω_p represents the rate at which proliferating cells undergo mitosis, ω_a represents the rate at which all live cells within the tumor undergo apoptosis (recall from the previous chapter that apoptosis has been shown to occur in all developed tumors), ω_n represents the rate at which dying cells in the necrotic region die, and finally ω_d represents the rate at which dead cells degrade and are removed from

the tumor. The parameters that were used in this model can be found in Table 1 and were also used as nominal values for the coupled model discussed in Section 3.2.2.

Table 1: Glioma Model Parameters

Parameter	Symbol	Values	Source
Nutrient Concentration outside the tumor	C_0	1.0 nmol/mm^3	[81]
Nutrient Concentration necessary for proliferation	C_h	$0.75xC_0$	[3]
Nutrient Concentration necessary to avoid necrosis	C_n	$0.5xC_0$	[82]
Diffusion Rate	D	12.96 mm^2/day	
Metabolic Consumption Rate	S	1786 nmol/mm^3·day	[83]
Radius of Glioma Cell	R_c	$5x10^{-3}$ mm	[84]
Proliferation Rate	ω_p	1/day	[82, 85]
Apoptosis Rate	ω_a	0.32/day	[82]
Necrosis Rate	ω_n	5/day	[3]
Degradation Rate	ω_d	0.05/day	[3]

It should be noted here that apoptosis is *controlled* cell death, as a result, degradation of cells which have undergone apoptosis occurs almost immediately, for the purposes of this model, it is assumed that such degradation is instantaneous. With Equations 16a and 16b, the model has been fully described, and has been expressed so that it may be solved using Runge-Kutta methods for the numerical solution of ordinary differential equations. An overview of this gliomas model is shown in Figure 3.

Model Overview

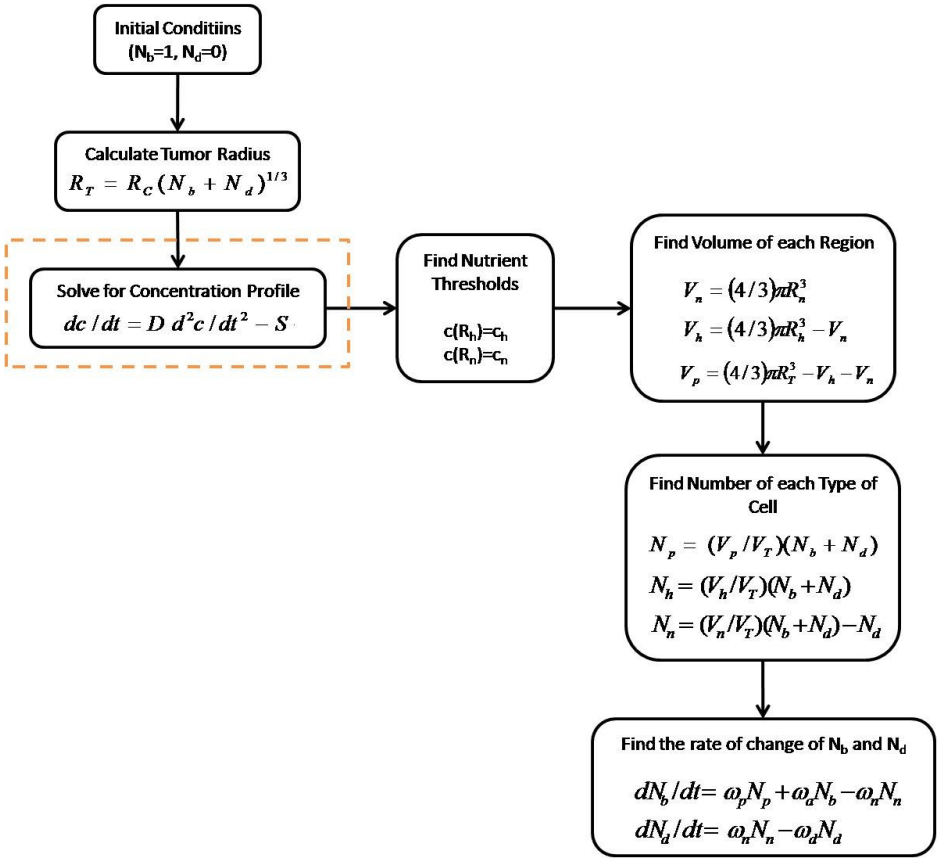

Figure 3: Glioma Model Overview

3.2.2 Coupled Tumorigenesis Model

In the case of a vascular tumor, the primary difference is that now there are sources of nutrients within the tumor, as opposed to merely outside the tumor (represented by the outer boundary condition in the avascular model). To allow for this an extra term was added to the partial differential equation governing the nutrient concentration in the tumor:

$$\partial c/\partial t = D_C \nabla^2 c - S + g\left(\varphi, c\right) \tag{17a}$$

$$g\left(\varphi, c\right) = 2\pi D_C R_{cap} \varphi f\left(r\right) \tag{17b}$$

$$f\left(r\right) = \left(c_b - c_b(R_T - r)/\delta\right)\left(1 - H(R_T - r - \delta)\right) \tag{17c}$$

where R_{cap} represents the radius of a capillary, δ represents the distance into the tumor where vascular affects remain significant, and *H(r)* represents the Heaviside step function. The term *g(φ,c)* represents the nutrient flux through the walls of the capillaries at a given point within the tumor, and depends upon the capillary length concentration and a predetermined nutrient concentration gradient across the capillary wall, *f(r)*, to account for the fact that the capillaries lose nutrients to the tumor; deeper locations will have less nutrients available, since much of the original nutrients have already diffused into the tumor. This decay in the capillary nutrient concentration gradient is important as it prevents a modeled tumor from growing exponentially without bound. The form of this gradient chosen is a linear decay from $c_{b,0}$ at the outside of the tumor to a value of zero at $r=\delta$. This choice was made for simplicity and ease of adjustability (the profile depends upon only one parameter), rather than being based upon any physical intuition. The form of *f(r)* is shown in Figure 4.

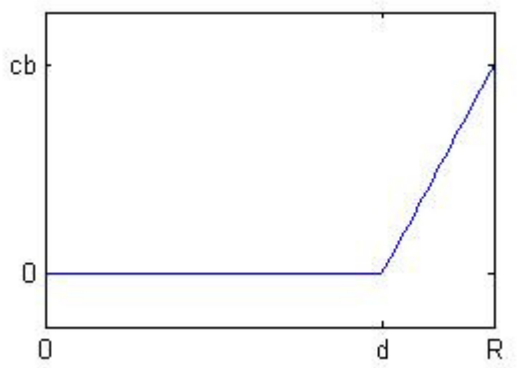

Figure 4: Form of the decay in the nutrient concentration gradient across the capillary wall. The gradient decays linearly up until some distance δ into the tumor, at which point the concentration within the capillaries has equalized with the nutrient concentration within the tumor, and the capillaries have no further effect.

By necessity, the capillary length density, *φ*, is solved for numerically, using a spatially discretized grid. As a result, a continuous solution is no longer applicable, and a discrete approach must be taken for obtaining the concentration profile. While the discretization of Equation 17 is relatively straightforward and will be discussed in the numerical methods section, solving for the unknown location of the inner boundary condition, *α*, requires a different approach than was taken previously

when α does not equal zero (i.e. there is a central region devoid of nutrients). In this case, an iterative process is undertaken where radial nodes are meshed on a domain bounded by (R_T,α), and values of ϕ are mapped onto these nodes through linear interpolation based upon the current solution. Then, the system of equations resulting from the discretization of the governing equation is solved to obtain a concentration profile. This iterative process is called using root finding methods to determine the value of α where the concentration gradient at $r=\alpha$ is zero, in which case the third condition in the avascular model is fulfilled. This process is demonstrated schematically in Figure 5.

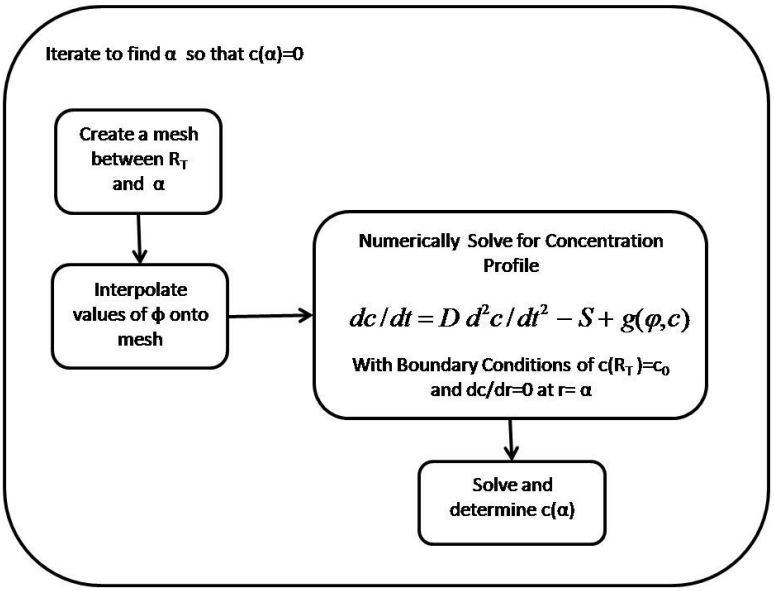

Figure 5: Iterative process for the solution of the equation governing the nutrient concentration in the vascular model when an inner region devoid of nutrients exists. An iterative root finder calls the solver for different values of α, seeking to find the value of α where the concentration at $r=\alpha$ is zero. (This replaces the boxed in portion on Figure 3.)

3.3 Angiogenesis Sub-model

3.3.1 Angiogenesis Model (Anderson & Chaplain[2])

As previously discussed, the starting point for the derivation of the angiogenesis sub-model is the seminal work by Anderson and Chaplain, who derived equations governing the migration of endothelial cells in angiogenesis. Although Anderson and Chaplain's work is discussed in the literature review, the equations are briefly discussed here as well. The model consists of three partial differential

equations, governing the rate of change of the endothelial cell concentration, n, angiogenic growth factor (AGF), c, and fibronectin, ρ:

$$\frac{\partial n}{\partial t} = \nabla \bullet \left[D\nabla n - n\left(\frac{\chi}{1+ac}\nabla c + \rho \nabla f \right) \right] \tag{18a}$$

$$\frac{\partial c}{\partial t} = -\eta n c \tag{18b}$$

$$\frac{\partial \rho}{\partial t} = \beta n - \gamma n f \tag{18c}$$

The terms in the equation governing the rate of change of endothelial cell concentration represent diffusion, chemotaxis, and haptotaxis, respectfully. These equations were originally derived to govern the migration of capillaries towards a static tumor that was yet to be influenced by the presence of the capillaries. As a result, multiple changes were required to develop a model appropriate for use in modeling the growth and development of a vascular tumor.

3.3.2 Coupled Angiogenesis Model

As previously discussed, haptotaxis was neglected in this model due to the symmetry of the model and haptotaxis' primary role of aiding anastomosis formation, which is neglected in the model. A major problem with this model for the purpose of deriving a model governing a vascular tumor is that the model has no memory of where endothelial cells (which can be used to represent the tip of an advancing capillary) have been in the past. Such knowledge is important in a vascular tumor model, since this represents where capillaries currently exist. As a result, the concepts of sprout tip concentration, s, and capillary length concentration, φ, were applied to the equations of Anderson and Chaplain. These concepts were developed by Balding and McElwain, whose work is also discussed in the literature review. Essentially, the use of these two variables splits the vascular state into the locations of

actively migrating sprout tips, represented by *s,* and the concentration of capillary that has been laid down by past migration, represented by *φ.* As capillaries are laid down in a region by the passage of sprout tips through the region, the rate of change of capillary length concentration is represented by the flux of sprout tips. Hence, the governing equations for the rate of change of sprout tip concentration and capillary length concentration are:

$$\frac{\partial s}{\partial t} = D_s \nabla^2 s - \nabla \bullet \left(\chi_0 s \nabla \{AGF\} \right) \tag{19}$$

$$\frac{\partial \phi}{\partial t} = D_s \nabla s - \chi_0 s \nabla \{AGF\} \tag{20}$$

Written in a spherical coordinate system and assuming symmetry, these equations reduce to:

$$\frac{\partial s}{\partial t} = \frac{D_s}{r^2} \frac{\partial}{\partial r} \left(r^2 \frac{\partial s}{\partial r} \right) - \frac{\chi_0}{r^2} \frac{\partial}{\partial r} \left(s r^2 \frac{\partial \{AGF\}}{\partial r} \right) \tag{21}$$

$$\frac{\partial \phi}{\partial r} = D_s \frac{\partial s}{\partial r} - \chi_0 s \frac{\partial \{AGF\}}{\partial r} \tag{22}$$

Note that as discussed in the model overview, the term for chemotaxis has been linearized for simplicity; in Anderson and Chaplain's model the chemotaxic coefficient is inversely proportional to the concentration of AGF, in addition to the dependence on the gradient of AGF.

Also resulting from Anderson and Chaplain's treatment of a static tumor, in the model a steady state AGF concentration profile was applied as an initial condition, which adjusted only due to increased uptake from migrating capillaries. However, in the case of a dynamic tumor, this is not the case; the AGF concentration must depend upon the tumor radius and, as it turns out, the nutrient concentration profile. As previously discussed, quasi-steady AGF concentration is assumed and calculated by Fickian

diffusion, with a source term *q(c),* which has a value of q_0 in hypoxic regions of the tumor, and is zero everywhere else. This is based upon the argument that proliferating cells are not starved of oxygen, while necrotic cells are dying and are no longer able to manufacture significant protein for signaling. The resulting equations and boundary conditions are:

$$\frac{\partial\{AGF\}}{\partial t} = D_{AGF}\nabla^2\{AGF\} + q(c) = 0 \tag{23a}$$

$$q(c) = \begin{cases} q_0 \text{ if } c_n < c < c_h \\ 0 \text{ if } c \le c_n \text{ or } c \ge c_h \end{cases} \tag{23b}$$

$$\left.\frac{dc}{dr}\right|_{r=0} = 0 \qquad c(\infty) = 0 \tag{23c}$$

The boundary conditions represent no flux through the tumors center and an infinite domain for the outer boundary condition (AGF can diffuse far past the outer domain of the tumor). These equations can be solved analytically in a manner similar to the nutrient concentration by dividing the equation into multiple domains. If no hypoxic region exists, the solution is trivial. Therefore there are two significant cases, one where there are two separate domains, representing the hypoxic region, and another representing the proliferating region as well as infinite surrounding tissue, and another where there is an additional inner domain of necrotic cells, which, like the proliferating cells, do not product AGF. To solve these equations, continuity of both the solution and the radial derivative of the solution is applied on the boundaries between separate domains.

3.4 Numerical Methods

3.4.1 Spatial Discretization

The model as present above consists of a series of nonlinear partial differential equations solved over a well defined geometry (symmetrical spherical). As a result, the chosen method for solving these

equations is finite difference discretization. A mesh of 400 nodes was created over the interval (0,R_T) towards this purpose. Equation 23a, which governs the nutrient concentration within the tumor, was discretized using a finite difference scheme as shown below to produce a linear system of equations, which can be solved using the methods of linear algebra:

$$\frac{\partial c}{\partial t} = \frac{D_c}{r^2}\frac{\partial}{\partial r}\left(r^2 \frac{\partial c}{\partial r}\right) - S + g(\phi, c) = 0 \tag{24}$$

As a first step, the outer derivative is approximated using a center difference:

$$D_c \frac{\left[r_{i+1/2}^2 \frac{dc(r_{i+1/2})}{dr} - r_{i-1/2}^2 \frac{dc(r_{i-1/2})}{dr}\right]}{\Delta r} - S r_i^2 + \frac{2\pi R_{cap} r_i^2}{D_c} f(r_i)(c_b - c_i) = 0$$

$$i = 2,3,\ldots n-1 \tag{25}$$

And in the second step, the inner derivative is approximated, remaining derivatives with center differences, to complete the discretization.

$$D_c \frac{\left[r_{i+1/2}^2 c_{i+1} - \left(r_{i+1/2}^2 + r_{i-1/2}^2\right)c_i + r_{i-1/2}^2 c_{i-1}\right]}{\Delta r^2} - S r_i^2 + \frac{2\pi R_{cap} r_i^2}{D_c} f(r_i)(c_b - c_i) = 0$$

$$i = 2,3,\ldots n-1 \tag{26}$$

These equations are applicable at every node except the innermost and outermost nodes, at which nodes equations are applied to enforce the boundary conditions. The discretized forms of the boundary conditions are:

$$\frac{dc}{dr} \approx \frac{c_1 - c_2}{\Delta r} = 0 \tag{27a}$$

$$c_n = c_0 \tag{27b}$$

Rearranging these terms to get all c_i on one side of the equation allows the system of equations to be written in matrix form:

$$[K]\{c\} = \{f\} \tag{28}$$

which can easily be solved by using the techniques of linear algebra. A similar discretization was performed for the angiogenesis equations, but the system of equations was arranged to solve for s_i^{j+1}, as will be described in the time discretization section.

3.4.2 Time

Examination of the systems of ordinary differential equations representing the tumorigenesis sub-model and a discretized angiogenesis sub-model (spatial discretization transforms a partial differential equation into a large system of ordinary differential equations) revealed that the equations representing the tumorigenesis sub-model are stable and step size was governed by accuracy requirements, while the equations representing the angiogenesis sub-model are unstable, or stiff, and step size using *explicit* solvers would be governed by stability requirements, instead of accuracy. As a result, over a given time step, the tumorigenesis sub-model was solved using a 2nd order explicit Runge-Kutta method, while the angiogenesis sub-model was solved using a 1st order implicit Runge-Kutta method (see Figure 6). This allowed maximum computational efficiency by using appropriate methods for each sub-model, since the form of the tumorigenesis model is not easily inverted to allow formulation of an implicit method, but the angiogenesis sub-model cannot efficiently be solved using explicit methods, due to instability.

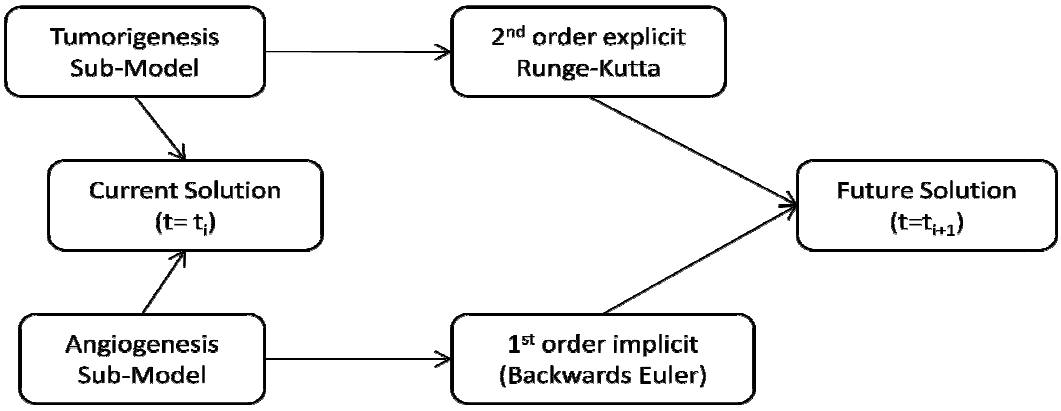

Figure 6: Schematic representation of the scheme of solution for solving the equations over time. The very nonlinear but stable tumorigenesis model was solved using 2nd order explicit methods, while the highly unstable but relatively linear angiogenesis model was solved using 1st order implicit methods. The two solvers ran simultaneously.

Chapter 4 Results

In this chapter, the results from the model are presented. In all cases the model was solved with an initial state of one live tumor cell, zero dead cells, and no active capillary sprout tips or existing capillaries ($s(r,0)=0$, $\varphi(r,0)=0$). Three major groups of results are presented below. First, the results from a sensitivity study are presented, the purpose of which is to study the sensitivity of the model to *local* changes in model parameter values around nominal values obtained from existing literature. Second, the results from a parametric study are presented. In contrast to the sensitivity study, the parameteric study gives insight into the affects of larger scale changes in parameter values on the solution. Finally, an optimization was performed to find the set of model parameters that best fit experimental data for tumor growth measured *in vivo* in a mouse model. The optimal solutions are presented, and the degree of agreement with the experimental results is characterized.

4.1 Sensitivity Study

A sensitivity study was performed to reveal which parameters have the most significant influence on tumor growth. This was conducted by perturbing each of seven model parameters

considered, which are presented in Table 3, by a small amount (0.1%) and observing the resulting change in the solution. This allowed estimation of the derivative dR_t/dq_i, where R_T represents the tumor radius and q_i represents a given model parameter. By examining the value of this derivative, one can observe the *e*ffects of *local* changes in the model parameter on the solution. The sensitivity of the tumor radius over time is presented in Figure 7a, and that of the number of live and dead cells in Figure 7b and Figure 7c, respectfully. This analysis revealed that the model is more sensitive to local changes in the tumorigenesis parameters (which are different from the angiogenesis parameters). The most sensitive tumorigenesis parameters are the proliferation rate, ω_p, and the degradation rate, ω_d, followed by the apoptosis rate, ω_a, and the nutrient diffusivity, D_c. In contrast, the length of the region influenced by angiogenesis, δ, and the sprout tip diffusivity, D_s, are among the least sensitive parameters. Increases in the proliferation rate result in increased tumor radius, while increasing the proliferation rate results in decreased tumor size. However, this analysis cannot provide any information about the effects of larger scale changes in the parameter values. For example, what affect does doubling the proliferation rate have on the model solution? Since the equations are nonlinear, the answers to such questions are not necessarily intuitive.

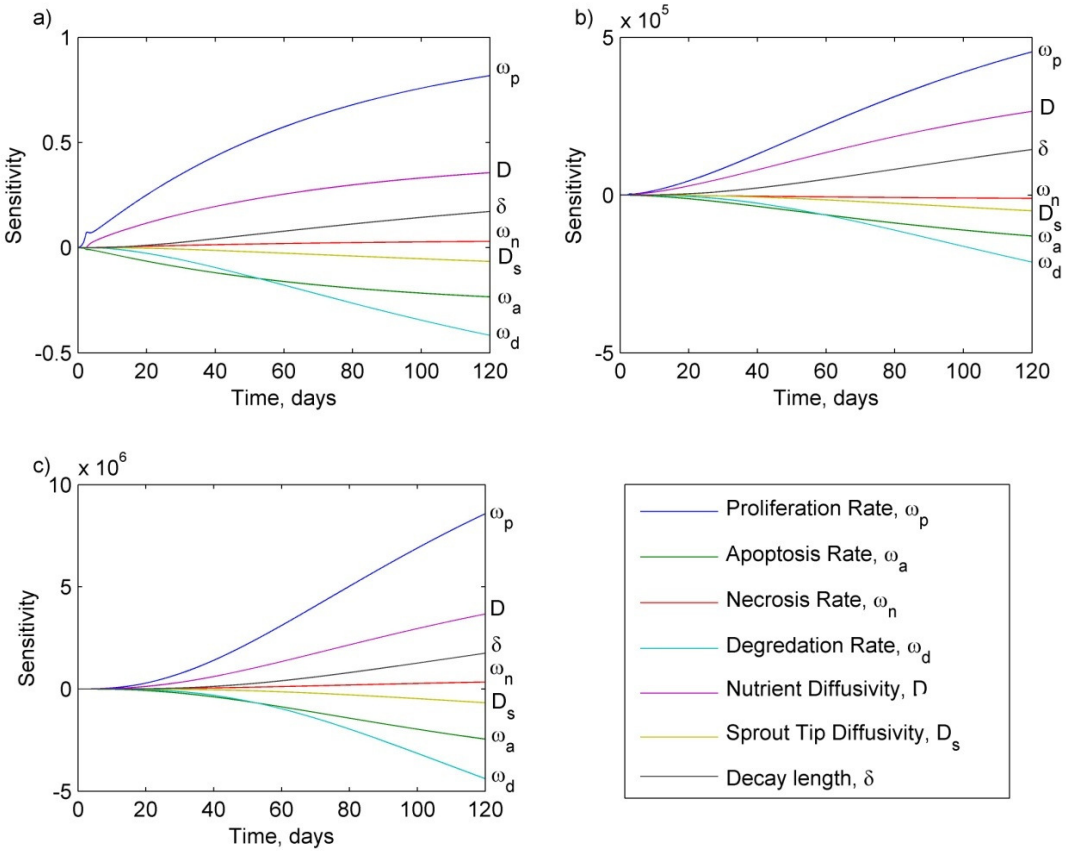

Figure 7: Sensitivity of the model predictions to local changes in the values of model parameters for: a) tumor radius, b) live cell count, and c) dead cell count.

4.2 Parametric Study

A parameteric study was performed to examine the affects of large scale changes in model parameters. To perform this study, the model was solved with the value of each model parameter being set at 1/10, 1/5, 5, and 10 times the nominal parameter value. This study showed that large scale changes in model parameters lead for the most part to relatively straightforward changes in the model solution, but there are several important exceptions. For increases in the proliferation rate, the instantaneous size of the tumor increases as would be expected, as shown in Figure 8. Also, the time required for the tumor size to plateau is reduced when the proliferation rate increases. Examination of Figure 8also shows that that if the proliferation rate is sufficiently reduced below a critical value the

tumor is unable to grow and shrinks to a zero radius. This behavior is due to the form of Equation 15a, which predicts the rate of change in the number of live cells present in the tumor. If the proliferation rate is smaller than the apoptosis rate, the tumor is unable to grow and eventually ceases to exist even if the tumor becomes sufficiently small so as to consist of only proliferating cells. This also demonstrates how increasing the apoptosis rate of tumor cells can lead to destruction of the tumor mass.

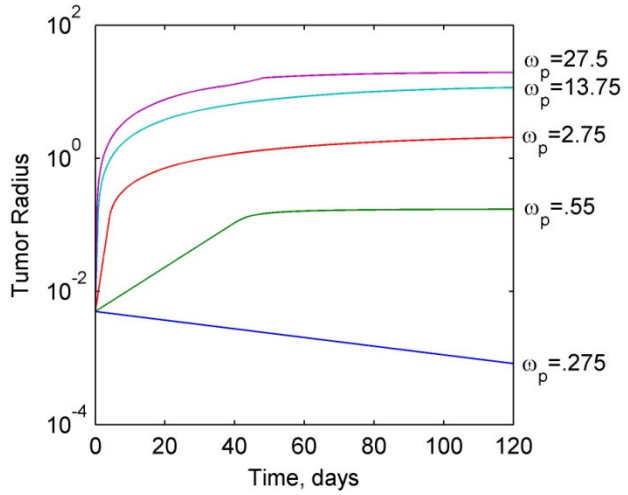

Figure 8: Response of the tumor growth predictions to variations in the proliferation rate ωp.

Increasing the degradation rate results in the tumor being unable to grow to sizes requiring a large necrotic core since any dead cells rapidly decay. On the other hand, decreases in the degradation rate result in increased tumor size, since more dead cells remain in the tumor body. As the degradation rate approaches zero, all dead cells are retained forever, and the tumor grows linearly without bound. These results are presented in Figure 9.

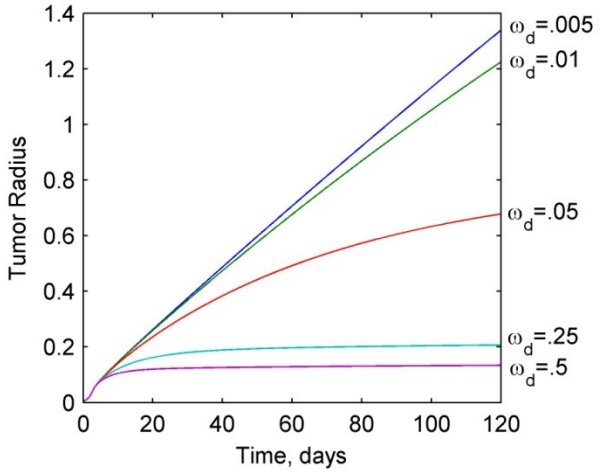

Figure 9: Response of the tumor growth predictions to variations in the degradation rate ωd.

Smaller, but still significant changes in the solution occur through changes in the value of the apoptosis rate and the nutrient diffusivity. For a sufficiently large apoptosis rate (that is greater than the proliferation rate) the tumor is unable to grow; this is the same affect that was observed in the results for the proliferation rate. This is a major physiological barrier to tumor development. For the opposite limiting case, when the apoptosis rate is negligible in comparison to the necrosis rate, the tumor grows rapidly but to a constant size due to cell necrosis and degradation, which ultimately will limit the size of the tumor even in the absence of apoptosis. These results are observed in Figure 10. On the other hand, increases in the nutrient diffusivity, D_c, steadily increase the tumor radius without bound. Nutrient diffusivities approaching zero result in a very small tumors, as shown in Figure 11, since nutrients fail to diffuse into the tumor (both from the surrounding tissue as well as the capillaries inside the tumor) quickly enough to keep up with the metabolic rate, S. Hence, the ratio of these two parameters is very important; this becomes clear from examining the form of Equation 24, as well as the work of Tanaka et al., where the vascular term was not present.

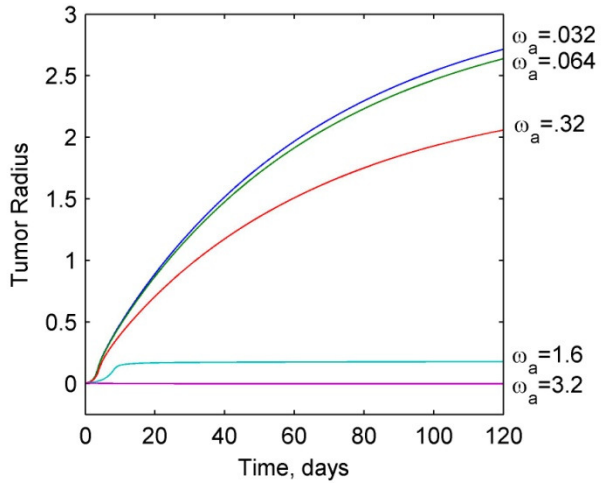

Figure 10: Response of the tumor growth predictions to variations in the apoptosis rate ωa.

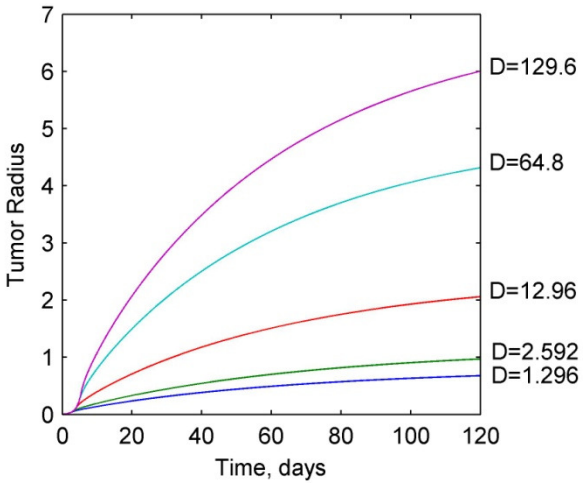

Figure 11: Response of the tumor growth predictions to variations in the nutrient diffusivity D_c.

The focus is shifted onto the interaction of angiogenesis and tumorigenesis in vascular tumors by examining the effects of large changes in the angiogenesis parameters (i.e., in the sprout tip diffusivity and the size of the affected region). As seen in Figure 12, an increase in the sprout tip diffusivity results in a corresponding increase in the tumor radius at any instant with the effect being relatively uniform over varying values of D_s. A twofold increase in the diffusivity, for instance, results in a 12% increase in the tumor radius at the end of the simulation, while a similar twofold decrease results in an 8% decrease in tumor size. This is in agreement with the results from the sensitivity study, where the

angiogenesis parameters generally had less affect on the model solution than the tumorigenesis parameters.

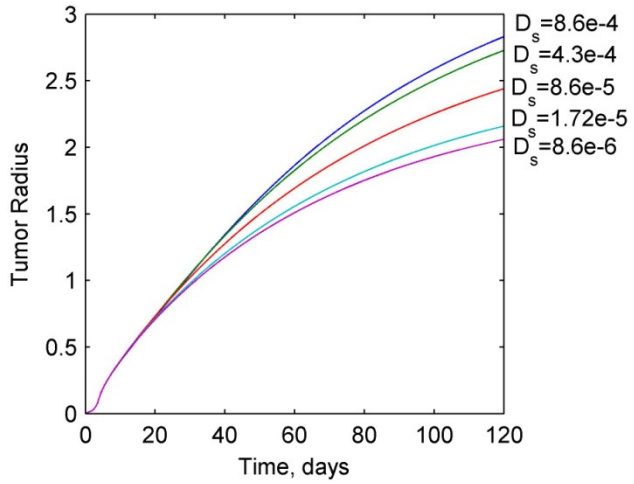

Figure 12: Response of the tumor growth predictions to variations in the sprout tip diffusivity Ds.

Large scale changes in the length of the affected region have a nonlinear influence on tumor size, and represent a distinct exception to the previous statement. For small values of δ, the predictions are similar to those for an avascular solution. However, as δ increases, the tumor size increases significantly. Indeed, unphysiologic behavior can be obtained by increasing this parameter by an order of magnitude. This is explained through Equation 17. The size of the affected region has no effect on the avascular nutrient concentration, since it only influences the nutrient concentration due to the capillaries. Hence, a sufficiently small affected region influences the nutrient concentration only in a small outer region of the tumor which is already well supplied with nutrients through the usual surface diffusion. As a result, the small local increase in nutrient concentration has little effect on tumor growth when δ is small. Thus, the solutions for the two smallest values of δ in Figure 13are virtually identical, and relatively close to the growth of an avascular tumor. This also explains the apparent disagreement between the sensitivity results, in which the affected length had comparatively little influence over the model solution, and this parametric study, where the parameter shows the ability to exert significant

influence over the solution. The use of an angiogenesis affected region in our model involves an *a priori* assumption about the nutrient concentration in the capillaries. A future approach could model the capillaries as flow tubes with nutrients diffusing out along its length in proportion to the external concentration, although this would increase the model complexity.

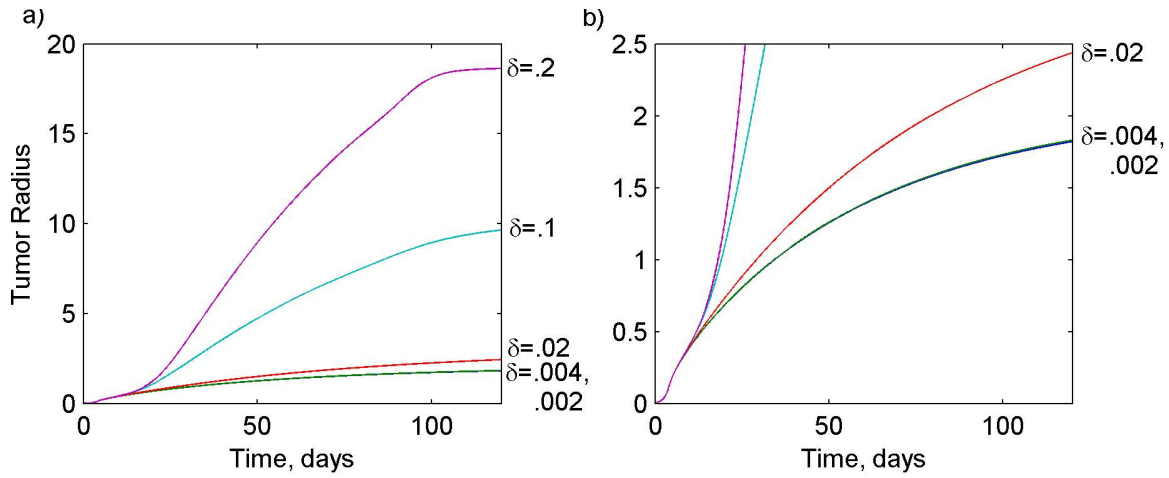

Figure 13: Response of the tumor growth predictions to variations in the various capillary nutrient concentration decay distances d.

4.3 Optimization and Optimal Results

The model was calibrated to fit it to experimental data available in the literature for human pancreatic tumor cell lines BxPC-3 and MiaPaCa-2[28], which were implanted in mouse models. In that study, real time quantitative measurements of the tumor volumes were obtained by imaging the tumors from different angles during its growth. This provided tumor volume data for eighteen implanted tumors from about 40 days up to about 140 days. Now the tumor radii predicted by the model can be compared with the average of the experimentally obtained tumor volumes. Although the determined optimal parameters are specific to the human pancreatic tumor data, the *framework* of the model should be valid for many different tumor types due to its fundamentally mechanistic nature.

For calibration, a weighting factor approach to optimize the initial model parameter values was used, such that the square of the difference between the experimental data and the predictions was minimized. Five model parameters were varied in the optimization: proliferation rate, ω_p, apoptosis rate, ω_a, necrosis rate, ω_n, sprout tip diffusivity, D_s, and the length of the region affected by angiogenesis, δ. The first three parameters represent the most sensitive model parameters, while the latter variables are the only parameters corresponding to the angiogenesis model. In the case of the length of the affected region, the parameter also showed the greatest influence over the model in the parametric study. These parameters are also listed in Table 3. Weighting factors were bounded in the range $0.1 < w_i < 10$. Hence, for each varied model parameter,

$$q_i = w_i q_{1,n} \tag{29}$$

where $q_{i,n}$ represents nominal values, which were obtained from the tumorgenesis[3] and angiogenesis[60] literature, and were used as the starting point for the optimization; these nominal parameter values can be found in Table 2. The weights were used as the variables in the optimization, which had the effect of normalizing the variations in all the variables, which simplified setting up the optimization problem. For the optimization, the cost function was taken to be the sum of the squared differences between the model solutions calculated with a specified set of parameter weights with respect to experimental data, toobtain a least squares solution, although due to the nature of the problem this cannot be performed through the familiar least squares regression. Instead, this optimization was performed in MATLAB using the function 'nonlinlsq', which performs nonlinear least squares optimization using an iterative approach.

The best fit solution is shown in **Error! Reference source not found.** along with the averaged xperimental measurements to which the model solution was fit. The calibration ratios corresponding to the best fit are shown in Table 3. There is good agreement between the model predictions and the

experiments (r^2 = 0.98). A key feature of the model is its ability to extrapolate early stage behavior that is not measureable through experiments such bioluminescence imaging experiments. The calibrated model for human pancreatic tumors was used to predicted tumor growth for both vascular and avascular tumors (shown in Figure 15). Although human pancreatic tumors are highly vascular, this approach allows us to understand the effect that vascularization has on tumor growth, thus providing insight into the underlying mechanisms. The model showed that the early behavior (prior to the development of a hypoxic region) of both vascular and avascular tumors is identical, which is to be expected, since in the absence of capillary length concentration (φ=0) the nutrient equation for the vascular tumor model reduces to that for an avascular tumor in the model of Tanaka et al. Beyond this early stage, avascular tumor growth begins to plateau due to limitations in the nutrient availability resulting from the balance of nutrient diffusivity and metabolic rate. Ultimately, a point is reached where the increase in the number of live cells due to proliferation is precisely matched by the rate of cell death in the necrotic region, which in turn matches the destruction rate of already dead cells in the necrotic core.

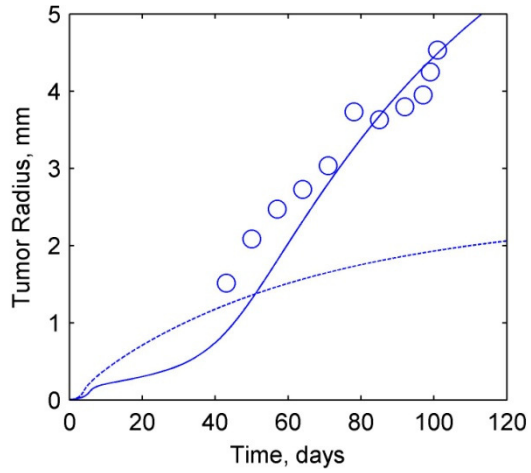

Figure 14: Comparison of experimental measurements from (31) and the 'best fit' model prediction resulting from the parametric study. The experimental data are available from ~40 days but most of the complexity in the predicted behavior occurs prior to this.

Table 2: Nominal parameter values used as the starting point for the optimization. Values for the tumorigenesis model parameters were obtained from Tanaka et al., values for angiogenesis model parameters were obtained from Anderson and Chaplain

Nomenclature	Symbols	Units
Nutrient Concentration	c	M/mm^3
Radial distance from tumor center	r	mm
Radius of tumor	R_T	mm
Radius of hypoxic shell	R_H	mm
Radius of necrotic core	R_N	mm
Time	t	days

Parameter	Symbols	Nominal Values	Calibrated Values	Units
Nutrient Concentration outside tumor	c_0	1		$nmol/mm^3$
Nutrient Concentration needed for proliferation	c_H	$0.75*C_0$		$nmol/mm^3$
Nutrient Concentration needed to avoid necrosis	c_N	$0.5*C_0$		$nmol/mm^3$
Cell Radius	R_c	0.005	-	mm
Nutrient Diffusivity	D	12.96	-	mm^2/day
Metabolic Rate	S	1786	-	$nmol/mm^3*day$
Proliferation Rate	ω_p	2.75	2.7626	1/day
Apoptosis Rate	ω_a	0.32	1.1091	1/day
Necrosis Rate	ω_n	5	1.1775	1/day
Degredation Rate	ω_d	0.05	-	1/day
Sprout Tip Diffusivity	D_s	0.00086	0.000115	mm^2/day
Chemotatic Constant	χ_0	22400000	-	$mm^2/nmol*day$
AGF Diffusivity	D_c	2.5	-	mm^2/day
Length of the affected region	d	0.02	0.0316	mm

Table 3: Calibration ratios corresponding to the best fit solution with the results of Bouvet et al.

Parameter	$w_i/w_{i,n}$
Proliferation Rate	1.0046
Apoptosis Rate	3.4658
Necrosis Rate	0.2355
Sprout Tip Diffusivity	0.1340
Length of the affected region	1.5790

On the other hand, a vascular tumor overcomes the nutrient limitation through transport from the capillaries so that its growth is not arrested, as shown in Figure 15a and Figure 15which present tumor radius and live and dead cell counts for both the vascular and avascular models. At the end of the simulation period of 120 days, the radius of the avascular tumor reaches a steady state radius of about 1mm, while the vascular tumor is still steadily growing due to the increase in capillary length concentration within the vascular tumor, due to the continued migration of sprout tips in response to AGF release by the hypoxic tumor cells. It is interesting to note that for both the avascular and vascular tumors, the vast majority of the cells in the tumor at the end of the simulation are dead. This is in clinical agreement with the necrotic cores commonly observed *in vivo.* It is also worth noting that dead cells do not appear until some finite time after the initiation of tumor growth, this corresponds to the development of a necrotic core.

The results for sprout tip concentration and capillary length concentration are shown in Figure 16a and Figure 16b, respectively**.** The invasion of microvessels into the tumor body is initiated on the tumor surface and intrudes inward into its mass over time. This intrusion is initiated at approximately the same time as the development of a hypoxic region within the tumor, since the process is triggered

through AGF release by hypoxic cells (as described in the theory section of this work). Ultimately, a uniform steady state sprout tip concentration profile is reached throughout the tumor volume (the simulation whose results are presented here did not proceed far enough in time for this steady state to be reached, however, this has been confirmed by other simulations). Meanwhile, the capillary length concentration has a maximum value on the outer edge of tumor and decreases linearly within the tumor until it reaches zero at the center. Due to the no flux boundary condition applied on the sprout tip concentration at the center of the tumor (again, as described in the theory section), and the fact that the capillary length concentration is calculated by determining the flux of the sprout tip concentration, the capillary length concentration in the center of the tumor must forever by zero. This is required to fulfill the inner boundary condition. This represents a limitation of the model, which results from the assumption of a spherically symmetric geometry that prevents successful (complete) angiogenesis from occurring. In a real tumor, of course, this inner boundary condition does not apply, and capillaries can develop even in the center of the tumor (which defines a state of successful angiogenesis), the conditions for which are discussed in the literature review. However, for the purposes of the model, the treatment of blood concentration gradient negates any affect from this symmetry assumption, since the concentration gradient across the wall of a capillary located at the center of the tumor would be zero.

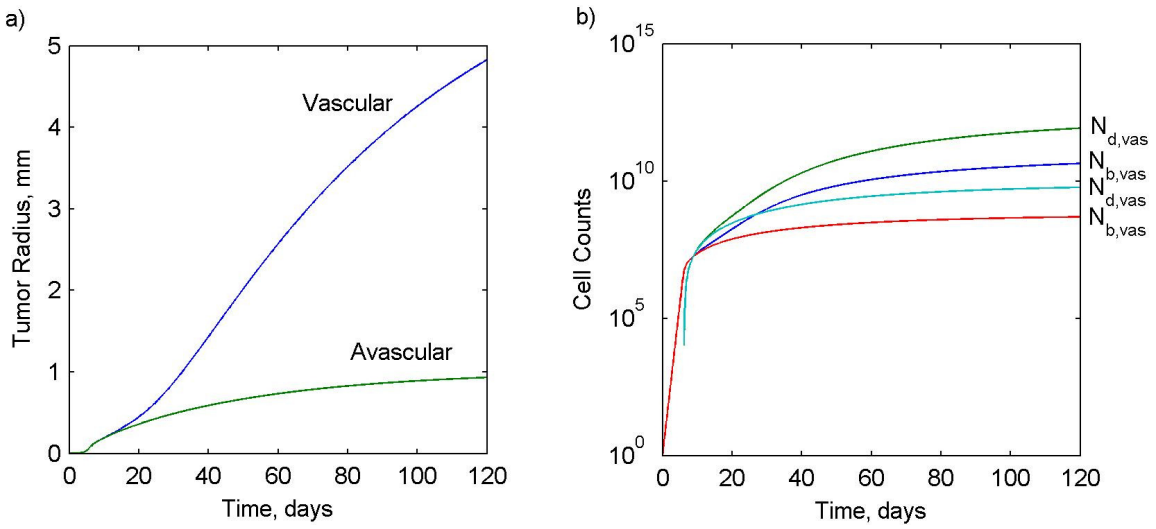

Figure 15: a) Predicted tumor radius of both a vascular and avascular tumors over 120 days. b) Live and Dead cell counts for both vascular and avascular tumors over the first 120 days following the onset of tumorgenesis.

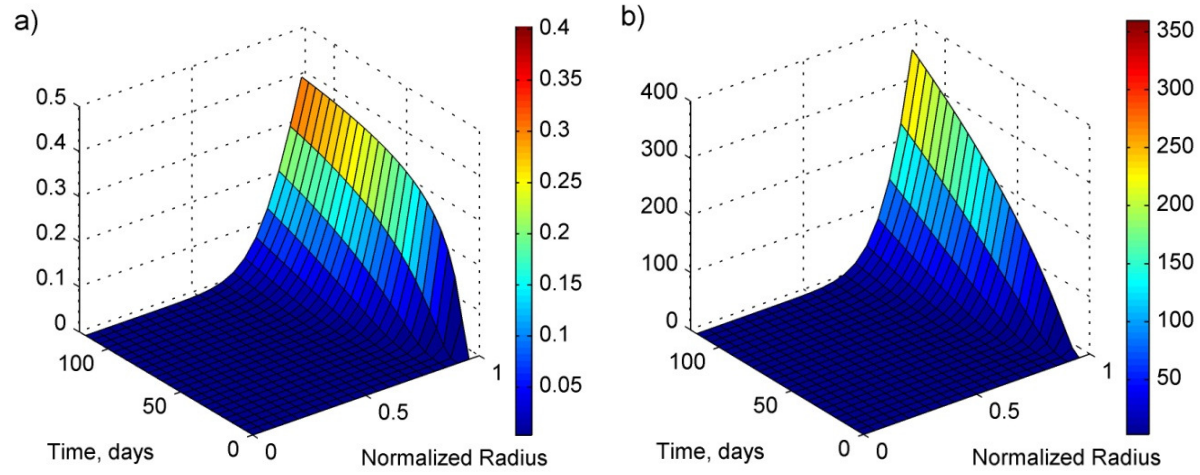

Figure 16: a) Sprout tip concentration within the vascular tumor. The sprout tip density is zero prior to the development of a hypoxic region at ~20 days. b) Capillary length concentration as a function of both normalized radius r/RT and time. This concentration is initially zero throughout the tumor but reaches a steady state and becomes a function of radius.

Chapter 5 Conclusions and Future Work

In this work, a relatively simple but mechanistic model of vascular tumor growth and development, derived in large part from prior works in the field, has been developed. In contrast to previous works modeling vascular tumor growth, the model makes relatively few assumptions regarding the behavior of the tumor (although certain aspects are neglected), particularly in comparison to other papers which assume *a priori* the state of vascularity. Analysis of the sensitivity of the model to both large and small scale changes in the model parameters has been presented, and the results demonstrate that the tumor response is for the most part more influenced by changes in the tumorigenesis model parameters, although large scale changes in the length of the angiogenesis affected region can have significant impacts upon the model solution.

The model has been validated through comparison with experimental results obtained through bioluminescence imaging of human pancreatic tumor in mouse models. An optimization routine was used to determine the set of model parameters that resulted in a best fit solution to the experimental data. Using these best fit parameters (which were limited to within one order of magnitude of published nominal values), a correlation coefficient of r^2=.98 was achieved, suggesting that the model is indeed capable of modeling real world tumors. Results for both tumor growth and angiogenesis progression from the optimal case solution are presented and discussed. It is important to note that due to the mechanistic nature of the model, it should be able to model most types of tumors, rather than being limited to pancreatic tumors alone.

Several available avenues for future work exist. In the model, the treatment of the nutrient concentration in the capillary blood within the tumor is empirical rather than mechanistic, one of the few components of the model that is not mechanistic. This assumption was made due to the complexity of modeling transport in such complicated networks, particularly under continuum assumptions where

knowledge of the precise capillary network is not available. Hence, one future avenue of inquiry would be the development of a continuum model of the nutrient and drug transport occurring due to the presence of capillaries within the tumor that is compatible with the continuum treatment of capillary length concentration presented in this work.

Another avenue of inquiry related to the first is to examine the effects of different treatment regimes on the behavior of the model. Completion of the previously proposed future research would allow for examination of the effects of chemotherapy on the model. An accurate model of transport within the capillary network is useful for such studies, since much of the tumor consists of already dead cells; concentrations of chemotherapeutic drugs need only be sufficiently high to reach those cells which are proliferating and quiescent in the outer regions of the tumor. Being able to quantify the dosage necessary to reach those cells more accurately may allow for reduced chemotherapy dosages, which obviously would be of great benefit to the patient given the severe side-effects of such drugs. A third avenue of inquiry would be the expansion of the model to consider the role of mechanical forces in the growth of the tumor.

Cancer remains one of the most significant health care challenges in the world today. Mathematical modeling of tumor growth and development allows greater insight into how to combat cancer in the most efficient manner possible, resulting in effective treatments and minimal side-effects for patients. It is hoped that the contribution of this body of work to the available literature may aid in these efforts, both extending the lives of many cancer patients and improving their quality of life.

References

1. *Society, A.C., Cancer Facts & Figures 2009. 2009, Atlanta, GA.*
2. *Anderson, A., Continuous and Discrete Mathematical Models of Tumor-induced Angiogenesis. Bulletin of Mathematical Biology, 1998.* ***60****(5): p. 857-899.*
3. *Tanaka, M.L., W. Debinski, and I.K. Puri, Hybrid mathematical model of glioma progression. Cell Proliferation, 2009.* ***42****(5): p. 637-646.*
4. *Hanahan, D. and R.A. Weinberg, The Hallmarks of Cancer. Cell, 2000.* ***100****: p. 57-70.*
5. *Fedi, P., S.R. Tronick, and S.A. Aaronson, Growth factors., in Cancer Medicine, J.R. Holland, et al., Editors. 1997, Williams and Wilkins: Baltimore, MD.*
6. *Lukashev, M.E. and Z. Werb, ECM signaling: orchestrating cell behaviour and misbehaviour. Trends Cell Biol, 1998.* ***8****: p. 437-441.*
7. *Giancotti, F.G. and E. Ruoslahti, Integrin signaling. Scienc, 1999.* ***285****: p. 1028-1032.*
8. *Medema, R.H. and J.L. Bos, The role of p21-ras in receptor tyrosine kinase signaling. Crit. Rev. Oncog. , 1993.* ***4****: p. 615-661.*
9. *Hanahan, D. and J. Folkman, Patterns and emerging mechanisms of the angiogenic switch during tumorigenesis. Cell, 1996.* ***86****: p. 353-364.*
10. *Wyllie, A.H., J.F. Kerr, and A.R. Currie, Cell death: the significance of apoptosis. Int. Rev. Cytol., 1980.* ***68****: p. 251-306.*
11. *Harris, C.C., p53 tumor suppressor gene: from the basic research laboratory to the clinic - an anbridged historical perspective. Carcinogenesis, 1996.* ***17****: p. 1187-1198.*
12. *Downward, J., Mechanisms and consequences of activation of protein kinase B/Akt. Current Opinion in Cell Biology, 1998.* ***10****(2): p. 262-267.*
13. *Cantley, L.C. and B.G. Neel, New insights into tumor suppression: PTEN suppresses tumor formation by restraining the phosphoinositide 3-kinase/AKT pathway. Proceedings of the National Academy of Sciences of the United States of America, 1999.* ***96****(8): p. 4240-4245.*
14. *Pitti, R.M., et al., Genomic amplification of a decoy receptor for Fas ligand in lung and colon cancer. Nature, 1998.* ***396****: p. 699-703.*
15. *Hayflick, L., Mortality and immortality at the cellular level. A review. Biochemistry, 1997.* ***62****: p. 1180-1190.*
16. *Wright, W.E., O.M. Pereira-Smith, and J.W. shay, Reversible cellular senescence: implications for immortalization of normal human diploid fibroblasts. Int. Rev. Cytol., 1989.* ***68****: p. 251-306.*
17. *Shay, J.W. and S. Bacchetti, A survey of teolmerase activity in human cancer. Eur. J. Cancer 1997.* ***33****: p. 787-791.*
18. *Bryan, T.M. and T.R. Cech, Telomerase and the maintenance of chromosome ends. Current Opinion in Cell Biology, 1999.* ***11****(3): p. 318-324.*
19. *Serrano, M., et al., Oncogenic ras provokes premature cell senescence associated with accumulation of p53 and p16. Cell, 1997.* ***88****: p. 593-602.*
20. *Bouck, N. and V.H. Stellmach, S.C., How tumors become angiogenic. Adv. Cancer Res., 1996.* ***69****: p. 135-174.*
21. *Folkman, J., Tumor angiogenesis, in Cancer Medicine, J.R. Holland, et al., Editors. 1997, Williams and Wilkins: Baltimore, MD. p. 181-204.*
22. *Kim, K.J., et al., Inhibition of vascular endothelial growth factor-induced angiogenesis suppresses tumour growth in vivo. . Nature, 1993.* ***362****: p. 841-844.*
23. *Millauer, B., et al., Gliblastoma growth inhibited in vivo by a dominant-negative Flk-1 mutant. Nature, 1994.* ***367****: p. 576-579.*
24. *Singh, R.K., et al., Interferons alpha and beta down-regulate the expression of basic fibroblast growth factor in human carcinomas. Proc. Natl. Acad. Sci. USA, 1995.* ***92****: p. 4562-4566.*
25. *Sporn, M.B., The war on cancer. Lancet, 1996.* ***347****: p. 1377-1381.*

26. *Christofori, G. and H. Semb, The role of the cell-adhesion molecule E-cadherin as a tumour-suppressor gene. Trends in Biochemical Sciences, 1999.* ***24****(2): p. 73-76.*
27. *Werb, Z., ECM and cell surface proteolysis: regulating cellular ecology. Cell, 1997.* ***91****: p. 439-442.*
28. *Bouvet, M., et al., Real-Time Optical Imaging of Primary Tumor Growth and Multiple Metastatic Events in a Pancreatic Cancer Orthotopic Model. Cancer Res, 2002.* ***62****(5): p. 1534-1540.*
29. *Jackson, T.L. and H.M. Byrne, A mathematical model to study the effects of drug resistance and vasculature on the response of solid tumors to chemotherapy. Mathematical Biosciences, 2000.* ***164****(1): p. 17-38.*
30. *Ganguly, R. and I.K. Puri, Mathematical model for chemotherapeutic drug efficacy in arresting tumour growth based on the cancer stem cell hypothesis. Cell Proliferation, 2007.* ***40****(3): p. 338-354.*
31. *Ganguly, R. and I.K. Puri, Mathematical model for the cancer stem cell hypothesis. Cell Proliferation, 2006.* ***39****(1): p. 3-14.*
32. *Bauer, A.L., T.L. Jackson, and Y. Jiang, A cell-based model exhibiting branching and anastomosis during tumor-induced angiogenesis. Biophysical journal, 2007.* ***92****(9): p. 3105–3121-3105–3121.*
33. *Mayneord, W.V., On a law of growth of Jensen's rat sarcoma. American Journal of Cancer, 1932.* ***16****: p. 841-846.*
34. *Haddow, The biological characters of spontaneous tumours of the mouse, with special reference to the rate of growth. J. Path. Bact., 1938.* ***47****: p. 553-565.*
35. *Thompson, R.H. and L.H. Gray, The histological structure of some human lung cancers and the possible implications for radiotherapy. British Journal of Cancer, 1955.* ***9****: p. 539-549.*
36. *Burton, A., Rate of growth of solid tumours as a problem of diffusion. Growth 1966.* ***30****(2): p. 157-76.*
37. *Greenspan, H.P., Models for the growth of a solid tumor by diffusion. Stud. Appl. Math, 1972.* ***51****(4): p. 317–340-317–340.*
38. *Sutherland, R.M. and R.E. Durand, Hypoxic cells in an in vitro tumour model. Int. J. Radiat. Biol, 1973.* ***23****: p. 235-246.*
39. *Durand, R.E., Cell cycle kinetics in an in vitro tumor model. Cell Tissue Kinet. , 1976.* ***9****: p. 403-412.*
40. *Kerr, J.F.R., A.H. Wyllie, and A.R. Currie, Apoptosis: a basic biological phenomenon with wide-ranging implications in tissue kinetics. British Journal of Cancer, 1972.* ***26****: p. 239-257.*
41. *McElwain, D.L.S. and L.E. Morris, Apoptosis as a volume loss mechanism in mathematical models of solid tumor growth. Math. Biosci. , 1978.* ***39****: p. 147-157.*
42. *Araujo, R.P. and D.L.S. McElwain, A history of the study of solid tumour growth: the contribution of mathematical modelling. Bulletin of Mathematical Biology, 2004.* ***66****(5): p. 1039–1091-1039–1091.*
43. *Roose, T., S.J. Chapman, and P.K. Maini, Mathematical models of avascular tumor growth. SIAM REVIEW, 2007.* ***49****(2): p. 179-208.*
44. *Düchting, W., A model of disturbed self-reproducing cell systems Biomathematics and Cell Kinetics, 1978.* ***2****: p. 133-142.*
45. *Düchting, W. and G. Dehl, Spread of cancer cells in tissues: Modelling and simulation. Int. J. Bio-Medical Computing, 1980.* ***11****: p. 175-195.*
46. *Düchting, W. and T. Vogelsaenger, Three-dimensional pattern generation applied to spheroidal tumour growth in a nutrient medium. Int. J. Bio-Medical Computing, 1981.* ***12****: p. 377-392.*
47. *Moreira, J. and A. Deutsch, Cellular Automation Models of Tumor Development: A Critical Review. Advances in Complex Systems, 2002.* ***5****(2/3): p. 247–268-247–268.*

48. *Kansal, A.R., et al., Simulated brain tumour growth dynamics using a three-dimensional cellular automaton J. Theor. Biology, 2000.* ***203****: p. 367-382.*
49. *Kansal, A.R., et al., Emergence of a subpopulation in a computational model of tumour growth. J. Theor. Biology, 2000.* ***207****: p. 431-441.*
50. *Dorman, G.D. and A. Deutsch, Cellular Automaton Modelling of Biological Pattern Formation. 2003, Boston: Birkhäuser.*
51. *Dresden, G., Modeling of self-organized avascular tumor growth with a hybrid cellular automaton. In Silico Biology, 2002.* ***2****(3): p. 393–406-393–406.*
52. *Jiang, Y., et al., A multiscale model for avascular tumor growth. Biophysical journal, 2005.* ***89****(6): p. 3884–3894.*
53. *Zawicki, D.F., et al., Dynamics of neovascularization in normal tissue. Microvascular Research, 1981.* ***21****: p. 27-47.*
54. *Balding, D. and D.L.S. McElwain, A mathematical model of tumour-induced capillary growth. Journal of Theoretical Biology, 1985.* ***114****: p. 53-73.*
55. *Byrne, H. and M. Chaplain, Mathematical models for tumour angiogenesis: Numerical simulations and nonlinear wave solutions. Bulletin of Mathematical Biology, 1995.* ***57****(3): p. 461-486.*
56. *Byrne, H.M. and M.A.J. Chaplain, Explicit solutions of a simplified model of capillary sprout growth during tumor angiogenesis. Applied Mathematical Letters, 1996.* ***9****(1): p. 69--74.*
57. *Orme, M.E. and M.A.J. Chaplain, A mathematical model of the first steps of tumour-related angiogenesis: capillary sprout formation and secondary branching. Mathematical Medicine and Biology, 1996.* ***13****(2): p. 73-98.*
58. *Orme, M.E. and M.A.J. Chaplain, Two-dimensional models of tumour angiogenesis and anti-angiogenesis strategies. Mathematical Medicine and Biology, 1997.* ***14****: p. 189-205.*
59. *Anderson, A.R.A. and M.A.J. Chaplain, A mathematical model for capillary network formation in the absence of endothelial cell proliferation. Applied Mathematical Letters, 1998.* ***11****: p. 109-114.*
60. *Anderson, A. and M. Chaplain, Continuous and discrete mathematical models of tumor-induced angiogenesis. Bulletin of Mathematical Biology, 1998.* ***60****(5): p. 857-899.*
61. *Chaplain, M.A.J., Mathematical modelling of angiogenesis. Journal of neuro-oncology, 2000.* ***50****(1): p. 37–51-37–51.*
62. *Mantzaris, N.V., S. Webb, and H.G. Othmer, Mathematical modeling of tumor-induced angiogenesis. Journal of Mathematical Biology, 2004.* ***49****(2): p. 111-187.*
63. *Anderson, A.R.A. and M.A.J. Chaplain, A gradient driven mathematical model of antiangiogenesis. Math. Comput. Modeling, 2000.* ***32****: p. 1141-1152.*
64. *Levine, H., et al., Mathematical modeling of capillary formation and development in tumor angiogenesis: Penetration into the stroma. Bulletin of Mathematical Biology, 2001.* ***63****(5): p. 801-863.*
65. *Levine, H.A., B.D. Sleeman, and M. Nilsen-Hamilton, Mathematical modeling of the onset of capillary formation initiating angiogenesis. Journal of Mathematical Biology, 2001.* ***42****(3): p. 195–238-195–238.*
66. *Ausprunk, D.H. and J. Folkman, Migration and proliferation of endothelial cells in preformed and newly-formed blood vessels during tumor angiogenesis. . Microvascular Research, 1977.* ***14****: p. 53-65.*
67. *Folkman, J., The vascularization of tumors. Sci. Am., 1976.* ***234****: p. 58-64.*
68. *Murray, J.D. and K.R. Swanson, On the mechanochemical theory of biological pattern formation with applications to wound healing and angiogenesis, in On Growth and Form: Spatio-Temporal Pattern Formation in Biology. 1999, Wiley: Chichester. p. 251-285.*

69. *Holmes, M.J. and B.D. Sleeman, A mathematical model of tumour angiogenesis incorporating cellular traction and viscoelastic effects. Journal of Theoretical Biology, 2000.* ***202****(2): p. 95–112-95–112.*
70. *Stokes, C.L. and L. D.A., Analysis of the roles of microvessel endothelial cell random motility and chemotaxis in angiogenesis Journal of Theoretical Biology, 1991.* ***152****: p. 377-403.*
71. *Othmer, H. and A. Stevens, Aggregation, blowup and collapse: The ABCs of taxis and reinforced random walks. SIAM Journal of Applied Mathematics, 1997.* ***57****: p. 1044-1081.*
72. *Paweletz, N. and M. Knierim, Tumor-related angiogenesis. Critical reviews in Oncology/Hematology, 1989.* ***9****: p. 197-242.*
73. *Patel, A.A., et al., A cellular automaton model of early tumor growth and invasion: the effects of native tissue vascularity and increased anaerobic tumor metabolism. Journal of Theoretical Biology, 2001.* ***213****(3): p. 315–331-315–331.*
74. *Hahnfeldt, P., et al., Tumor Development under Angiogenic Signaling A Dynamical Theory of Tumor Growth, Treatment Response, and Postvascular Dormancy 1. Vol. 59. 1999: AACR.*
75. *Jackson, T.L., Vascular tumor growth and treatment: Consequences of polyclonality, competition and dynamic vascular support. Journal of Mathematical Biology, 2002.* ***44****(3): p. 201–226.*
76. *McDougall, S.R., et al., Mathematical modelling of flow through vascular networks: implications for tumour-induced angiogenesis and chemotherapy strategies. Bulletin of mathematical biology, 2002.* ***64****(4): p. 673–702-673–702.*
77. *Netti, P.A., et al., Time-dependent behavior of interstitial fluid pressure in solid tumors: implications for drug delivery. Cancer Res, 1995.* ***55****: p. 5451-5458.*
78. *Netti, P.A., et al., Macro- and microscopic fluid transport in living tissues: application to solid tumors. AIChE J., 1997.* ***43****: p. 717-734.*
79. *Hogea, C.S., B.T. Murray, and J.A. Sethian, Simulating complex tumor dynamics from avascular to vascular growth using a general level-set method. Journal of Mathematical Biology, 2006.* ***54****: p. 86-134.*
80. *Frieboes, H.B., et al., An Integrated Computational/Experimental Model of Tumor Invasion. Cancer Res, 2006.* ***66****: p. 1597-1604.*
81. *Gruetter, R., et al., Direct measurement of brain glucose concentrations in humans by 13C NMR spectroscopy. Proc. Natl. Acad. Sci. USA, 1992.* ***89****: p. 1109-1112.*
82. *Frieboes, H.B., et al., Computer simulation of glioma growth and morphology. Journal of theoretical biology, 2007.* ***245****: p. 677-704.*
83. *Spence, A.M., et al., Glucose metabolism in human malignant gliomas measured quantitatively with PEt, 1-[C-11]glucose and FDG: Analysis of the FDG lumped constant. Journal of Nuclear Medicine, 1998.* ***39****: p. 440-448.*
84. *Swanson, K.R., et al., Virtual and real brain tumors: using mathematical modeling to quantify glioma growth and invasion. Journal of the neurological sciences, 2003.* ***216****(1): p. 1–10-1–10.*
85. *Stein, A.M., et al., A mathematical model of glioblastoma tumor spheroid invasion in a three-dimensional in vitro experiment. Biophysical journal, 2007.* ***92****: p. 356-365.*